ENGINEERING SITE INVESTIGATION OF SOIL COMPETENCE WITHIN MOUNTAIN TOP UNIVERSITY'S PERMANENT SITE AT MAKOGI-OBA, OGUN STATE, USING GEOPHYSICAL METHODS

By

AGBONJARU DAVID CHUKWUEBUKA

16010401004

A PROJECT SUBMITTED TO THE DEPARTMENT OF GEOSCIENCES, COLLEGE OF BASIC AND APPLIED SCIENCES, MOUNTAIN TOP UNIVERSITY, PRAYER CITY, OGUN STATE, NIGERIA

IN PARTIAL FULFILMENT OF THE REQUIREMENTS FOR THE AWARD OF BACHELOR OF SCIENCE (B. Sc.) DEGREE IN GEOPHYSICS

DECEMBER, 2020

DECLARATION

I hereby declare that this project has been written by me and is a record of my own research work. It has not been presented in any previous application for a higher degree of this or any other University. All citations and sources of information are clearly acknowledged by means of reference.

_____

AGBONJARU, DAVID CHUKWUEBUKA

_____

Date

CERTIFICATION

This is to certify that the content of this project entitled "**Engineering site Investigation of Soil Competence within Mountain Top University's Permanent Site at Makogi-Oba, Ogun State, Using Geophysical Methods"** was completed and submitted by **AGBONJARU, DAVID CHUKWUEBUKA** with matriculation number 16010401004, in partial fulfilment of the requirements for the award of **BACHELOR OF SCIENCE (B.Sc.) DEGREE IN GEOPHYSICS**. The original research work was carried out by him under my supervision and is hereby accepted.

PROFESSOR ELIJAH A. AYOLABI _____

Supervisor *(Signature and Date)*

DR. O. B. BALOGUN _____

Supervisor *(Signature and Date)*

DR. O. B. BALOGUN _____

Head of Department *(Signature and Date)*

DEDICATION

I dedicate this thesis to God, the creator of the universe, and my family.

ACKNOWLEDGEMENTS

I am much grateful to the ALMIGHTY GOD for the grace and prolonged fortitude, in not only enabling me to complete this thesis but also for the successful completion of the degree. I would like to appreciate the university for providing the equipment used for the data acquisition. My profound gratitude goes to the Vice-Chancellor, Prof. E.A. Ayolabi, for his tremendous support and assistance. I will like to use this medium to appreciate the efforts of my Supervisor, Dr O.B. Balogun for without his consistent persuasion and patience in dealing with me, I wouldn't be completing this research project. I also very especially grateful to the member of staffs of Geosciences Department Dr. J.A. Adeoye, Mr. M.O. Okunnubi, Mr. R.P. Akinwale, Mr. Dayo O. Ebun and Mr. A. O. Alao, right from the onset of the project, down to fieldwork, data processing and completion of the entire write-up.

My dearest family, I am ever-bound to your numerous supports and contribution towards my formal education, and also for your motivation. I want to thank my father, in the person of Mr. Sunday Agbonjaru for financing the project and playing a pivotal role during the fieldwork. My dear colleague, a friend, a brother, Omishakin Solomon A., you surprised me and exceeded my expectations numerously. I remember what you said: "all things will fall into place subsequently". I appreciate your effort in putting me through the various aspect from the fieldwork to processing software. I would also like to thank Mr. Emmanuel whose is currently doing his M.Sc., Mr. Segun, Uncle Maxwell and Mr. Akeem who made themselves readily available for the fieldwork. Onimisi ThankGod thanks for your advice.

TABLE OF CONTENTS

CHAPTER FOUR

RESULTS AND DISCUSSION

LISTS OF FIGURES

Figures **Pages**

LISTS OF TABLES

ABSTRACT

Geophysical methods have been used to investigate the competence of the near surface soil at Mountain Top University's permanent site in Makogi-Oba, via Ibafo, Lagos-Ibadan Expressway, Ogun State, Nigeria with a view to determining its suitability for construction purposes.

The methods adopted include the 2D electrical resistivity tomography, 1D Vertical Electrical Sounding, 2D seismic refraction tomography and the multichannel analysis of surface wave. The 2D ERT was first conducted and this was followed by the Vertical Electrical Sounding at some selected points on the 2D ERT profiles. This was followed by the seismic refraction tomography survey before the multichannel analysis of surface waves was finally done.

The 2D electrical resistivity imaging delineated between three to four layers which were the clayey top soil, a clayey sand layer, a low resistivity clay and another clayey sand layer. Maximum depth probed was 49.7 m. The Vertical Electrical Sounding delineated four geoelectric layers which were interpreted as clayey topsoil, a clay layer, clayey sand layer and a bottom clay layer. From the vertical electrical soundings, top soil resistivity and depth ranged from 12 to 51 ohm-m and 0.4 to 0.8 m respectively, second layer resistivity and depth ranged from 3 to 7 ohm-m and 1.5 to 5.2 m respectively, third layer resistivity and depth ranged from 13 to 163 ohm-m and 1.6 and 9.1 m respectively. The fourth layer resistivity varied between 3 to 46 ohm-m. Though just relatively competent, the third layer is the most competent layer delineated and depth to this layer ranged between 2.2 and 5.6 m. On the seismic survey models, only two distinct layers were delineated with the discrimination property being the degree of consolidation of the earth materials. Seismic compressional wave velocity, shear wave velocity, bulk density, compressibility, bulk modulus, shear modulus and rock-mass quality within the first layer ranged between 511 and 1500 m/s, 175 and 185 m/s, 1.474 and 1.929 gcm^{-3}, 0.235 x 10^{-6} and 3.150 x 10^{-6} Pa, 0.318 x 10^{6} and 4.262 x 10^{6}

Pa, 52,349 and 55362 Pa, and 0.001026 and 0.01 respectively. Within the second layer, seismic compressional wave velocity, shear wave velocity, bulk density, compressibility, bulk modulus, shear modulus and rock-mass quality ranged between 1042 and 1750 m/s, 230 and 240 m/s, 1.761 and 2.005 gcm^{-3}, 0.167 x 10^{-6} and 0.546 x 10^{-6} Pa, 1.832 x 10^{6} and 5.993 x 10^{6} Pa, 96519 and 110728 Pa, and 0.003484 and 0.01778 respectively.

The study identified the clayey sand layer as the most competent lithologic layer within the near subsurface sequence and concluded that the near surface strata in their present state are not competent to bear the load of heavy engineering construction. It is recommended that a pile foundation which could be anchored in the clayey sand layer be considered in case the site is to be developed. It should be noted however that before any construction of any sort should be done at this site, the mechanism to take care of flooding that occurs when the Ogun river dam is spilled out should be put in place.

CHAPTER ONE

INTRODUCTION

1.1 General Introduction

Mountain Top University is a developing institution of higher learning which has continued to grow rapidly since its inception. The growth has been rapid that its present campus is becoming congested and there is now the undeniable need for expansion.

In reaction to this, the University has procured a bigger expanse of land, known as the permanent site, where minor construction activity has commenced. However, before extensive construction activities can commence, it has become necessary that geophysical investigations which will be complementary to the suites of geotechnical investigation that have been done be carried out.

The role of geophysicist in engineering sites investigations cannot be overemphasised and it keeps evolving (Adewunmi and Olorunfemi, 2005). Geophysics offers a reliable, rapid and non-invasive approach to investigating the earth's near-surface. It has also proved to be effective in assessing the condition of sub-grade soil (Momoh *et.al*., 2008). Unfortunately, it has not found general acceptance in civil engineering practices partly due to the fact it is an evolving practice and partly because conventional civil engineers feel threatened by it.

While geophysics has not been recommended solely as the means of investigating the soil for engineering practice, integrating it with geotechnical methods have the benefit of compensating for the deficiencies of geotechnics, one of which its failure to be able to detect sub-surface geologic structures which could be inimical to heavy engineering structures. It is therefore in an effort to have a comprehensive and holistic understanding of the nature and competence of near-surface soil within Mountain Top University permanent site that this project was conceived. We want to build structures that will be strong, durable and safe at the permanent site.

1.2 Study Area

1.2.1 Description of Study Area

The study area is the proposed university library at Mountain Top University's permanent site in Makogi-Oba community, off Lagos-Ibadan Expressway, Ibafo area, Ogun state, Nigeria. With reference to the WGS'84 datum, the area falls between latitudes 06.7472701^{o} N and 06.7501100^{o} N; and longitudes 03.3811654^{o} E and 03.3835190^{o} E (Figure 1.1). Expressed in Universal Transverse Mercator (UTM) coordinates with reference to WGS'84 datum, the area is delimited by latitudes 745827 and 7456141 mN; and longitudes 542122 and 542382 mE. The area is a plain with elevation ranging between 7.5 and 18.5 m above the mean sea level (Figure 1.2).

1.2.2 Relief, Climate and Vegetation

1.2.2.1 Relief

The area is a gently undulating lowland where many beels are present. Elevation ranges between 7.5 and 18.5 m. The major river draining the region is River Ogun.

1.2.2.2 Climate

The region experiences two climatic seasons which are the dry and wet seasons. The dry season spans from November to March, and the wet season from April to October (Adeleke and Leong, 1978). Available rainfall data shows that rain falls throughout the whole year but a noticeable sharp decrease is usually observed from November to March. Average rainfall is 1693 mm per year while average temperature is 27.0ºC (Climate-data.org, 2020).

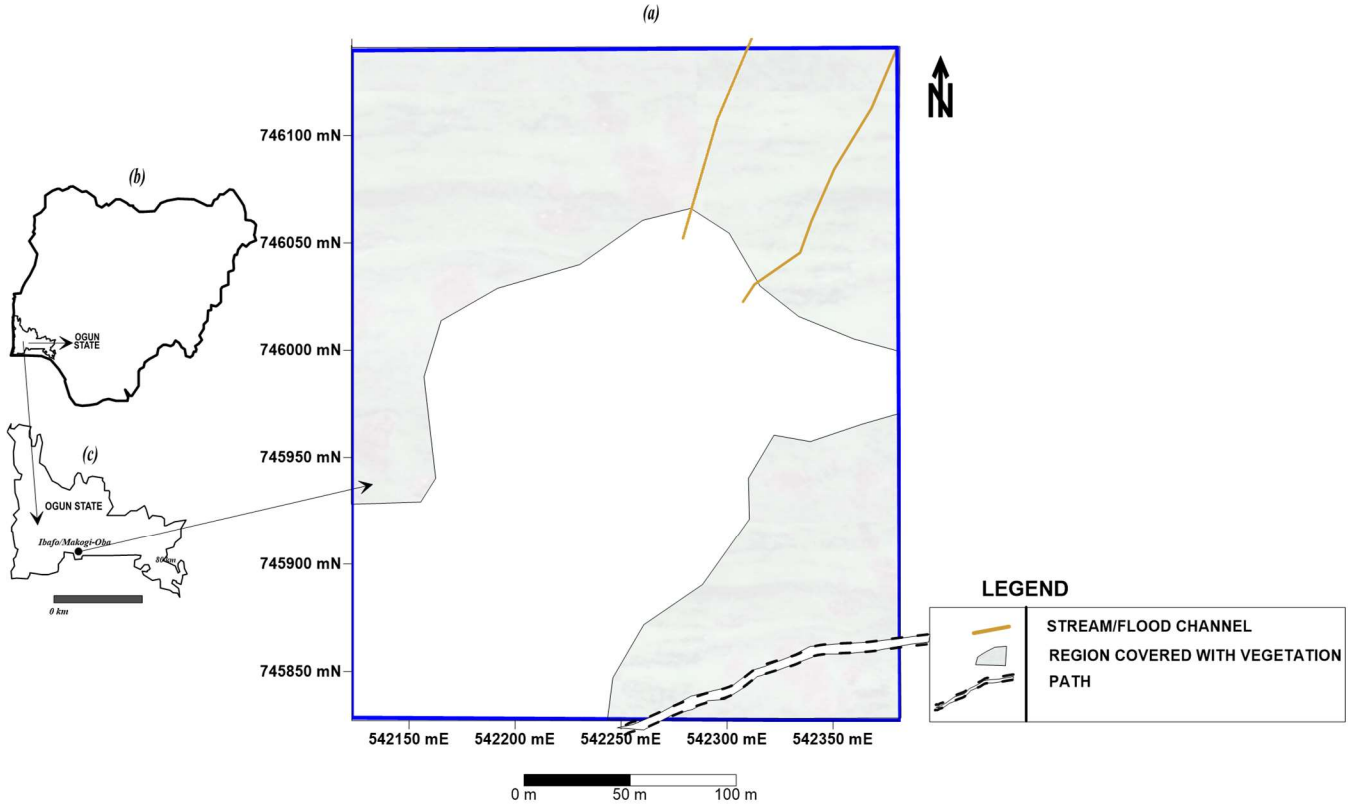

Figure 1.1: Location map of (a) the study area (b) Nigeria showing Ogun state (c) Ogun state showing Ibafo/Makogi-Oba. *(Digitised after Google Maps, 2020)*

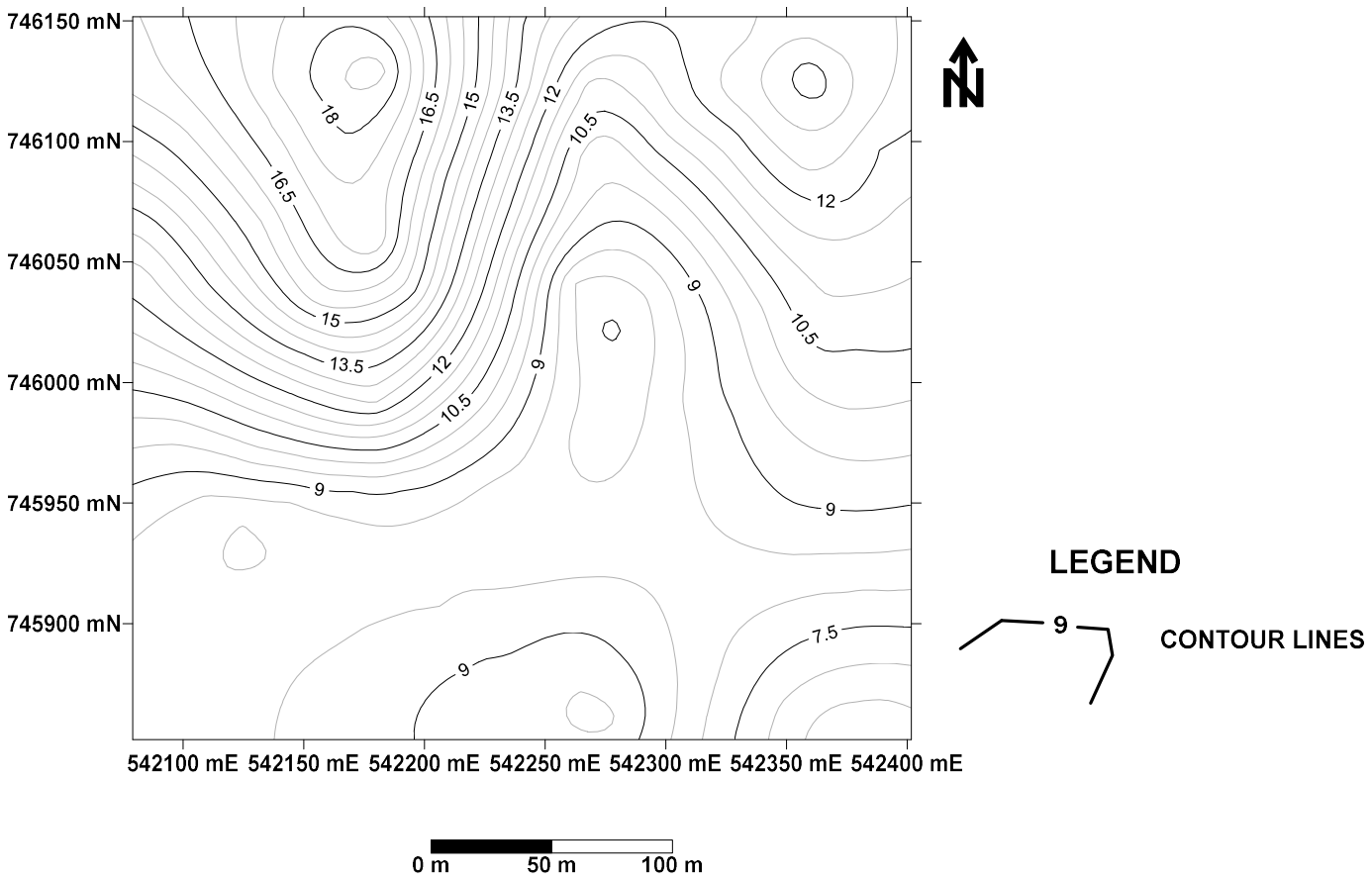

Figure 1.2: Elevation Map of the Study Area *(Obtained from SRTM (USGS, 2006))*

1.2.2.3 Vegetation

Ibafo (Makogi-Oba) is a wetland region. The vegetation of Ibafo is very similar to the vegetation observed generally in Lagos state, Nigeria. Just as in Lagos state, the vegetation can be classified as a typical swamp forest consisting of freshwater regions/freshwater swamp forest (Lagos state government). In the flood plain regions, only grasses that are tolerant of heavy water are present.

1.2.3 Geology of the Study Area

1.2.3.1 Regional Geology of the Study Area

The study area falls within the western section of the Nigerian sector of the Dahomey basin. The basin was believed to have been formed in response to the separation of South America from Africa during the Mesozoic (de Klasz, 1978). The oldest sediments in the basin, known as Ise Formation, are non-fossiliferous, folded rocks of unknown thickness but pre-Albian (early Cretaceous) in age. The youngest strata are Pleistocene to Recent in Age. The strata deposited during the Cretaceous were assigned to the Abeokuta Group by Omatsola and Adegoke (1981) and subdivided into three formations which were the Ise Formation (oldest), Afowo Formation, and Araromi Formation (youngest). Overlying the Araromi Formation is the Ewekoro Formation which is also overlain in places where they occur by the Oshosun Formation.

1.2.3.2 Local Geology of the Study Area

The study area lies within the Recent Alluvium and Coastal Plain Sands of the Nigerian sector of the Dahomey Basin, Southwestern Nigeria (Figure 1.3).

1.2.3.3 Hydrogeology of the Study Area

The study area is within the floodplain of the Ogun river, with a tributary of the river within the University. The area is prone to flooding.

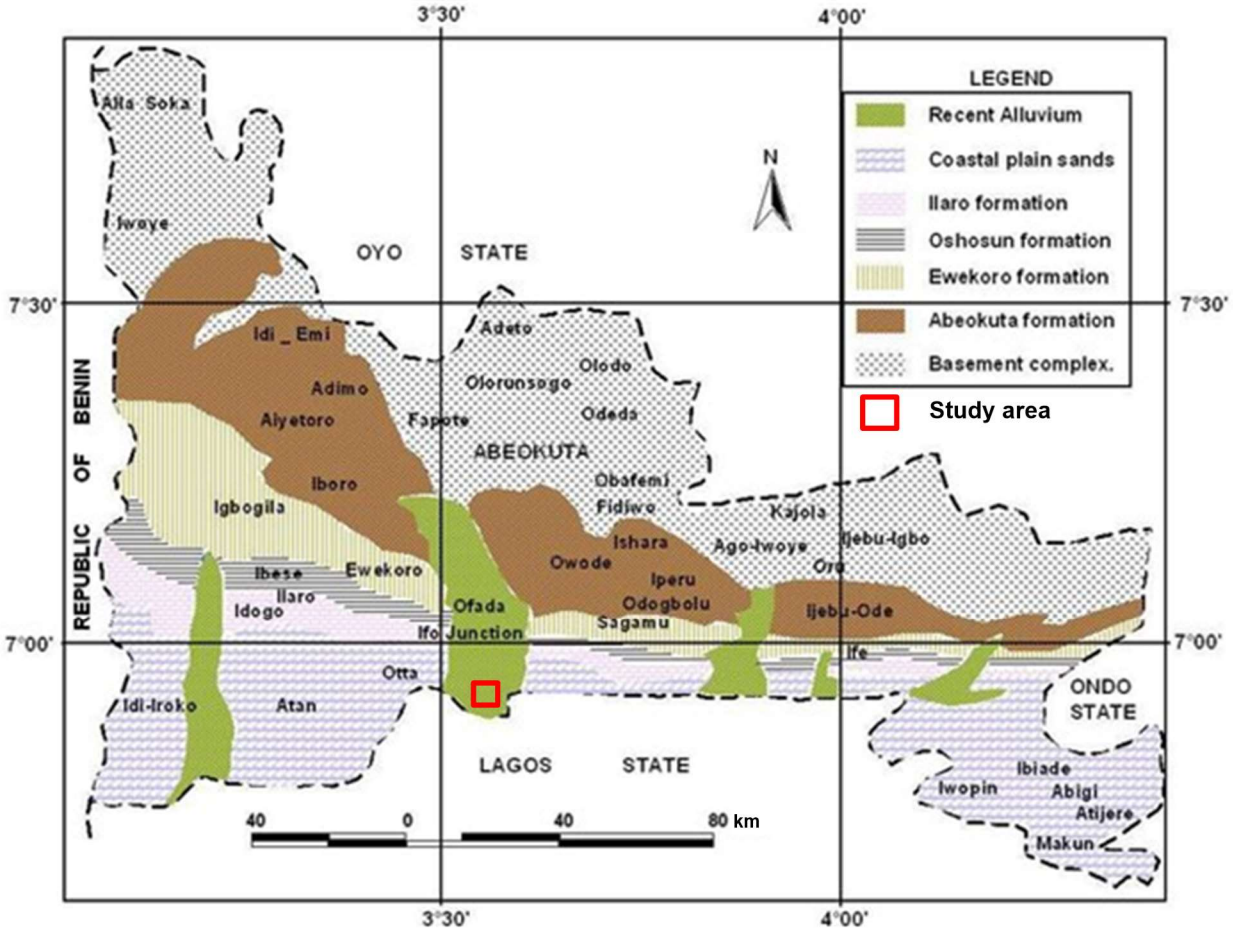

Figure 1.3: Geologic Map of the Nigerian Sector of the Dahomey Basin (After Petters, 1982).

Inset is the study area.

1.3 Problem Definition

Construction activities associated with large scale urbanization has been on the rise in Nigeria. A lot of these construction activities have involved the siting of large engineering structures which are expected to be strong, durable and safe for use. There has however been an increasing trend in the rates of failure of such engineering structures. Most of the time, the design of these structures is faultless but they still fail because comparably less attention is given to the study of soil competence and investigations about the presence of geologic structures which could be dangerous to such large engineering structures.

Therefore, to prevent the issue of failure of erected buildings and other engineering structures that will be sited, engineering site investigation of the soil competence and near-surface geological structures within Mountain Top University permanent site was done so that necessary precautions can be taken when construction commences in earnest.

1.4 Aim and Objectives of the Study

The aim of the study is to determine the suitability of the near subsurface soil for construction of engineering structures using integrated geophysical and geotechnical methods.

The specific objectives are as follow:

i. to evaluate the competence of the sub-surface layers at the near-surface using geophysical methods.
ii. to investigate the presence of near-surface geologic structures that could be inimical to engineering structures.
iii. to make recommendations on remediation modalities if potential threats to engineering structures were identified.

1.5 Literature Review

Geophysics is a science discipline that helps us discriminate and characterise earth materials based on their contrasting physical properties which may include electrical conductivity (or resistivity), magnetic susceptibility, rate of propagation of seismic waves, composition of natural radioactive materials etc., (Adewumi and Olorunfemi, 2005; Momoh *et.al.,* 2008). These authors were also able to establish that relationship exist between competence of earth materials and their physical properties (Adewumi and Olorunfemi, 2005; Momoh *et.al.,* 2008). Geophysics helps to reveal the presence of contrasting geophysical properties of earth material in situ in a minimally invasive and rapid manner, thereby providing accurate data from which competence of earth materials can be evaluated. In addition, the configuration of bedrock and presence of geologic structures (some of which could be inimical to engineering structures) and their prospective influence can be evaluated (Adepelumi and Olorunfemi, 2000; Momoh *et.al.,* 2008; Akintorinwa and Adeusi, 2009; Ayolabi *et al.,* 2012).

According to Adewumi and Olorunfemi (2005), geophysical studies of engineering sites before construction is highly relevant and can be used to derive qualitative information about the condition of the subsurface and competence of soil. Geophysical methods can be utilized independently or in mixes for engineering site analysis (Adewumi and Olorunfemi, 2005; Ayolabi *et al,* 2012). The utilizations of such geophysical method include evaluation of depth to bedrock and determining bedrock configuration, assessment of the competence of subgrade soils and mapping of underground geological structures (Akintorinwa and Adeusi, 2009; Adepelumi and Olorunfemi, 2000). Geophysics provide a rapid, non-invasive and cost-effective means of assessing the competence of soil for suitability for engineering construction purpose (Momoh *et.al.,* 2008).

As a rapid means of rock identification and site selection in foundation design and construction of engineering structures, the direct current resistivity method is particularly effective (Adewumi and Olorunfemi, 2005). 2D and 3D Electrical Resistivity Tomography (ERT) are excellent for imaging bedrock topography and structures in areas of relatively thin overburden as in a typical basement complex terrain. They also give excellent result when applied in sedimentary basins and coastal areas for engineering site investigation (Ayolabi *et al.,* 2012). The technique of vertical electrical sounding (VES) may be used to investigate the subsoil of a site in terms of the water table, the characteristics of the soil, the extent, the depth and distribution of each soil type, and even the consistency of the soil type in relation to engineering works (Adewumi and Olorunfemi, 2005; Ayolabi *et al.,* 2012). Integration of geotechnical methods with geophysical methods to investigate engineering sites is often encouraged because geotechnical investigation results provide a typical benchmark against which the geophysical results can be evaluated especially in cases where doubt could arise due to lack of relevant priori information. In addition, both geophysical and geotechnical investigations are known to be complementary to one another (Adewumi and Olorunfemi, 2005).

Ayolabi et al. (2012) integrated 2D electrical resistivity tomography, cone penetrometer test (CPT) and standard penetration test (SPT) in order to pinpoint the proficient subsurface layer for the foundation of engineering structures. The result proved the method as very efficient in identifying competent and less competent earth materials. It also proved beyond doubt the importance of conducting thorough geophysical and geotechnical before erecting engineering structures.

1.6 Research Methodology

Existing literatures relevant to the study were first reviewed. This was followed by reconnaissance site visit and generation of the basemap for the study area. Field data acquisition plan was then

designed. Geophysical methods adopted were the 2D electrical resistivity tomography (ERT), 1D vertical electrical sounding (VES) technique of the electrical resistivity method, 2D seismic refraction tomography and the multichannel analysis of surface wave (MASW).

The 2D ERT was first conducted, this was followed by the VES along selected points on the 2D ERT profiles. The VES has the capacity to better resolve adjacent beds that may have appeared merged on a 2D ERT inverted section. Following the VES survey, were the 2D seismic refraction tomography and the MASW surveys.

Though, the inherent disadvantage of seismic refraction tomography is that it does not resolve adjacent sedimentary layers optimally (in sedimentary terrains) compared to when it is being used to map basement – overburden boundary (in basement complex terrains), it still remains the only method that can give us elastic and acoustic parameters (e.g., bulk modulus, shear modulus, Poisson's ratio and Lame's constant) relating to soil competence. Subsurface (geologic) structures that could pose any form of threat to engineering structures are expected to be revealed on the ERT imaging sections and the VES geoelectric sections.

The 1D VES was expected to better resolve vertical beds with less superimposition, approximation or suppression of individual bed layers as could happen in seismic refraction and electrical resistivity tomography. While the best picture of the subsurface is better gotten from ERT imaging, layer thicknesses and their respective apparent resistivity values which could be used to infer the competence of each geologic layer are better gotten from 1D VES.

1.7 Limitation of the Study

Geotechnical (soil) test data such as lithologic logs, Standard Penetration Test, Cone Penetration Test and the Atterberg limit tests were not available to constrain the geophysical interpretation.

1.8 Expected Contribution to Knowledge

The research is expected to reveal to us the degree of competence of the soil at the near surface and to as well reveal the presence of any geologic structures that may be dangerous to the siting of any proposed engineering structure.

The research is also expected to give recommendations to remediate any unfavorable soil conditions based on the result of the investigation.

CHAPTER TWO

BASIC THEORIES AND PRINCIPLES OF THE GEOPHYSICAL METHODS USED

2.1 The Geophysical Methods

Geophysical methods are very versatile and have the ability to measure physical properties contrast such as electrical resistivity (or conductivity), magnetic susceptibility, density, acoustic impedance e.t.c. in earth materials and this has made them suitable for various studies such as mapping of geologic boundaries (or structures), determination of depth to bedrock (or competent earth material), evaluation of fluid saturation within the sub-surface as well as delineating various geologic layers that make up the lithological succession in a terrain. The principles of the geophysical methods used in this study are discussed in this section.

2.2 The Electrical Resistivity Method

This method employs the use of direct, artificially generated current, which is introduced into the ground and measures the resulting potential difference at the surface (Telford *et al.,* 1990; Kearey *et al.,* 2002). Deviation from the pattern of potential differences expected from homogenous ground provides information on the form and electrical properties of subsurface. The electrical resistance of the ground is determined by the introduction of electrical current (I) into the ground by means of electrodes called the current electrodes and measuring the corresponding potential difference generated via the potential electrodes also driven into the ground (Reynolds, 1997). Thus, the apparent resistivity of the ground is further calculated from the measured parameters: resistance and geometric factor of the electrode array used, using the relation:

$$\ell_a = \frac{\Delta v}{I} \mathrm{K} \qquad 2.1$$

$$R=\frac{\Delta v}{I} \quad 2.2$$

$$\ell_a=RK$$

where k = Geometric Factor

2.2.1 Definition and Units of Resistivity

It is well known that the resistance R in ohms of a wire is directly proportional to the length L, and is inversely proportional to its cross-sectional area A that is:

$$R \propto {}^{L}/_{A} \quad 2.3$$

$$R = \ell {}^{L}/_{A} \quad 2.4$$

where ℓ, the constant of proportionality, it is known as the electrical resistivity or electrical specific resistance, a characteristics or electrical specific resistance, a characteristic of the material which is dependent of its shape or size. According to ohm's law, the resistance is given by

$$R = \frac{\Delta V}{I} \quad 2.5$$

Where ΔV is the potential difference across the resistance and I is the electrical current through the resistance. Substituting equation 2.5 into equation 2.4 we have

$$\frac{\Delta V}{I} = \ell\frac{L}{A} \quad 2.6$$

Cross multiplying, we have

$$I\ell L = \Delta vA \quad 2.7$$

Making ℓ the subject of the formulae we get

$$\ell = \frac{A}{L}\frac{\Delta v}{I} \qquad 2.8$$

In a semi-infinite material the resistivity at every point must be defined. If the cross-sectional area and length of an element within the semi-infinite material are shrunk to infinitesimal size then the resistivity, ℓ, may be defined as follows,

$$\ell = \frac{\lim_{L\to 0}\frac{\Delta V}{L}}{\lim_{A\to 0}\frac{I}{A}} \qquad 2.9$$

Recall; $E = \frac{V}{L}$ and $J = \frac{I}{A}$

$$\ell = \frac{E}{J} \qquad 2.10$$

Where E is the electrical field and J is the current density.

$$J = \frac{E}{\ell}$$

But $\sigma = \frac{I}{\ell}$

Therefore, $J = \sigma E$ 2.11

Where σ is the conductivity of the material. The unit of resistivity is the ohm-meter (Ω-m)

2.2.2 Potential Distribution within the Earth

According to Telford et al., (1990) and Reynolds (1997), the earth is assumed to be a homogenous body in which potential distribution at any point within it is the same (Figures 2.1 and 2.2).

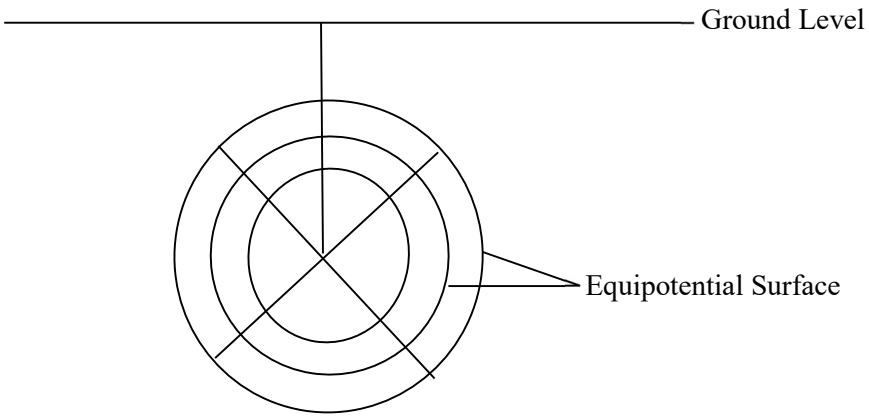

Figure 2.1: Radial Current Flow within a Homogeneous Earth (After Telford *et al.,* 1990)

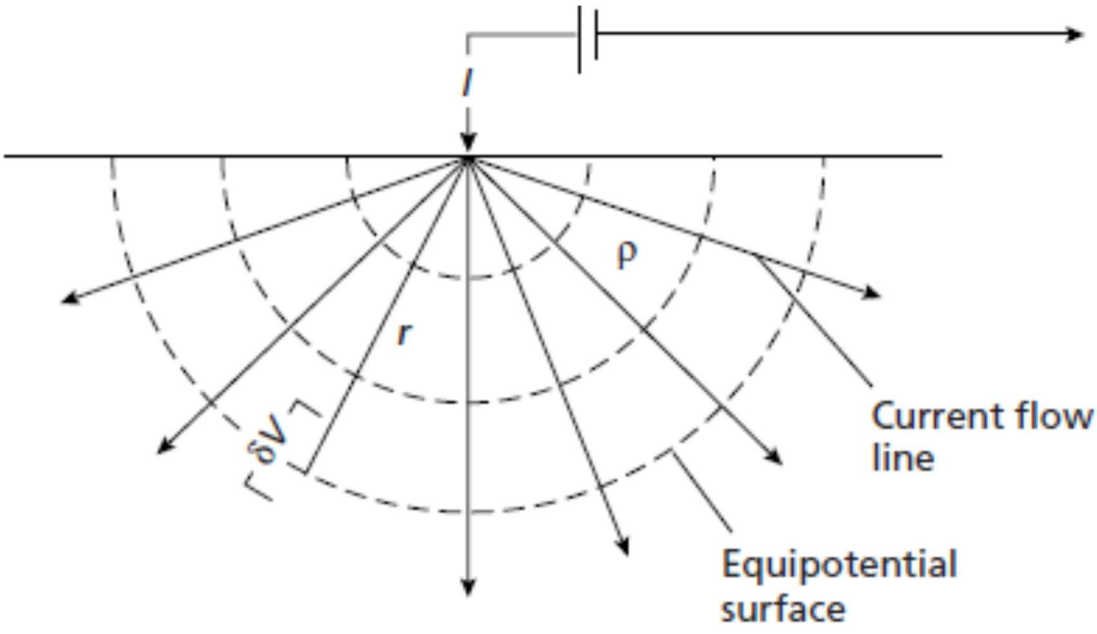

Figure 2.2: Radial Current Flow in a Hemispheric Earth (After Telford *et al.,* 1990)

$$J = \frac{I}{A} = \frac{I}{4\prod r2} \quad 2.12$$

Since area of a sphere = $4\pi r^2$

But $J = \sigma E$

$$\sigma E = \frac{I}{4\pi r^2} \quad 2.13$$

$$\frac{\sigma \partial v}{\partial r} = \frac{I}{4\pi r^2}$$

$$\partial v = \frac{I}{\sigma} \frac{I}{4\pi r^2} \partial r$$

$$\partial v = \ell \frac{I}{4\pi r^2} \quad 2.14$$

On integrating both sides we have,

$$V = -\ell \int \frac{I}{4\pi r^2} \partial r$$

$$V = \frac{\ell I}{4\pi r} \quad 2.15$$

Equation 2.15 gives the electrical potential V at any point P caused by a point electrode emitting an electrical current (I) in an infinite homogenous and isotropic medium of resistivity ℓ. In contrast to equation 2.15 and general assumption, the earth is semi-infinite and in homogenous in practice. Thus, the current source is located at the surface of hemispherical earth (Figure 2.2).

$$J = \frac{I}{A}$$

But the cross-sectional area for a hemisphere is $2\pi r^2$

$$J = \frac{I}{2\pi r^2}$$

$$- \frac{\sigma \partial v}{\partial r} = \frac{I}{2\pi r^2} \quad 2.16$$

$$\partial \mathrm{v} = \frac{\partial I}{2\pi r^2} \partial \mathrm{r}$$

$$\int \partial \mathrm{v} = - \ell \int \frac{I}{2\pi r^2} \partial \mathrm{r}$$

$$\mathrm{V} = \frac{\ell I}{2\pi r} \quad 2.17$$

2.2.3 Geometric Factor and Apparent Resistivity due to a Point Current Source

In practice a potential difference rather than a potential is measured and four electrodes are mostly used. According to Telford et al., (1990). The geometric factor due to the specific array configuration are computed so that apparent resistivity which is the product of the geometric factor and resistance can be calculated. The apparent resistivity equation for the four-electrode system is derived below (Figure 2.3). It should be noted that Geometric factors are not affected by interchanging current and voltage electrodes but voltage electrode spacing are normally kept small to minimize the effects of natural potential (Telford *et al.*, 1990)

Potential at M due to A is

$$V_M{}^A = \frac{\rho I}{2\pi}\left[\frac{1}{R_A} - \frac{1}{R_B}\right] \quad 2.18$$

Potential at N due to B is

$$V_N{}^B = \frac{\rho I}{2\pi}\left[\frac{1}{R_A} - \frac{1}{R_B}\right] \quad 2.19$$

Absolutely potentials are difficult to monitor so the potential difference ΔV between electrodes C and D is measured as shown in equation (2.20),

$$\Delta V = V_M - V_N = \frac{\rho I}{2\pi}\left\{\left[\frac{1}{r_A} - \frac{1}{r_B}\right] - \left[\frac{1}{R_A} - \frac{1}{R_B}\right]\right\} \quad 2.20$$

Thus, equation (2.8) can be written for ρ as stated in equation (2.21),

$$\rho = \frac{2\pi \Delta V}{I\left[\left[\frac{1}{r_B} - \frac{1}{r_B}\right] - \left[\frac{1}{R_A} - \frac{1}{R_B}\right]\right]} \quad 2.21$$

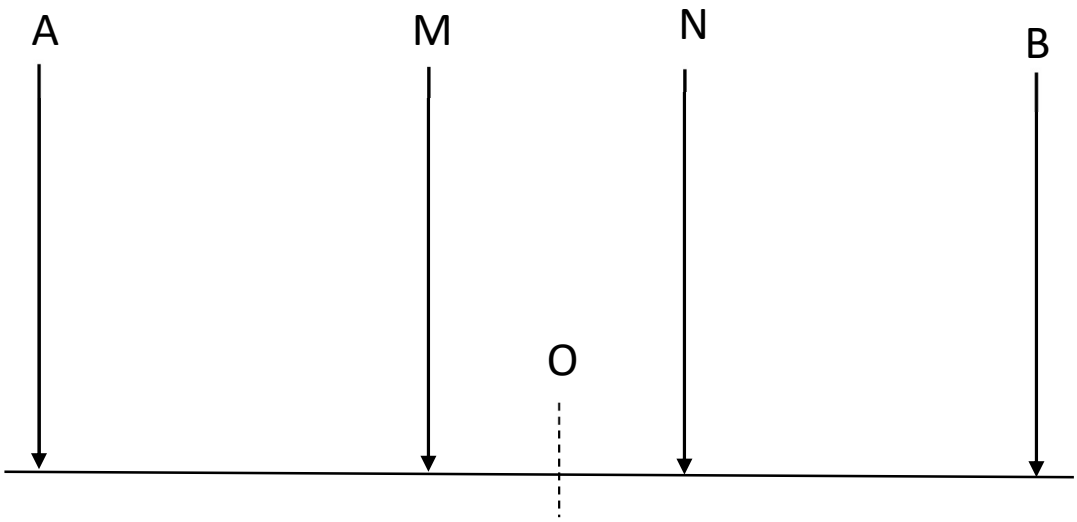

Figure 2.3: A Four Electrode system (After Telford *et al.,* 1990)

2.2.4 The Multielectrode System Configuration

The arrangement of electrodes in relation to each other is called the electrode configuration. Wenner, Schlumberger, dipole-dipole, gradient, pole-pole, pole-dipole and squared array are some of the array types that exist (Loke, 2002). Traditionally, all of these arrays make use a pair of current and potential electrodes, but technology has made it available that we can have numerous electrodes which are selected in pairs of current and potential electrode automatically. This is the concept of multielectrode system configuration. All the various array type used in traditional 2D electrical resistivity survey can also be engaged in the multielectrode system configuration.

2.2.5 Limitations of Electrical Resistivity Method

The interpretation of a multiplayer sounding curve generally is not unique (Kearey *et al.,* 2002). This means that a given electrical sounding curve can correspond to a variety of subsurface distributions of layers' thicknesses and resistivities. Furthermore, several other limitations are inherent in the conventional methods of electrical sounding (Telford *et al.,* 1990; Kearey *et al.,* 2002). They are:

(i) Equivalence: This occurs in multi-layer resistivity curve. The curve can correspond to a great number of different geoelectric models. Commonest types of equivalence problem are:

   a. equivalence of K-type curves

   b. equivalent of H-type curves.

(ii) Monotonic change in resistivity: When the resistivity of the subsurface layer increases and decreases monotonically, the sounding curve may resemble a curve of a simple two-layer earth

model (principle of suppression), unless the thickness of the layers increases significantly with depth.

(iii) Relative thickness of a layer: The detectability of a layer of given resistivity depends on its relative thickness which is defined as the ratio of the bed thickness to its depth of burial. The smaller the relative thickness of a given layer the smaller the chance of its detectability on a sounding curve.

2.2.6 Field Operational Problem

Field operational problems associated with electrical resistivity method are:

(i) Poor Electrode/Ground Contact: Electrical contact may be poor and hence conductivity reduced, if the ground is hard and dry, ambiguous reading can be generated, thus the ground has to be moisturized to improve the ground conductivity.

(ii) Lateral inhomogeneity: Lateral inhomogeneity of the earth can disrupt the quality of data.

(iii) Dip effect: If the dip is less than 10^{o}, then its gently dipping interface, therefore the effect is considered insignificant. But when the dip is greater than 10^{o} it gently affects the degree of accuracy of data generated.

Noise: These are unwanted signals generated by interference e.g., Telluric noise, Power lines, buried pipes e. t. c.

2.3 Seismic Refraction Method

Seismic waves are energy waves that pass through the layers of the earth, resulting from earthquakes, volcanic eruptions, magma movement, massive landslides, and large man-made explosions that emit acoustic energy at low frequency (Reynolds, 2011). Short-lived wave trains, known as pulses, which usually contain a broad range of frequencies, are produced by sources suitable for seismic surveying. The seismic pulse propagation speeds are determined by the elastic moduli and densities of the materials through which they move (Telford *et al*., 1990; Kearey *et al.,* 2002; Reynolds, 2011).

There are two main types of seismic waves: those that pass through the bulk of a medium are known as body waves while those confined to the interfaces between media with contrasting elastic properties, particularly the ground surface, are called surface waves. The body waves can further be categorized into two namely:

1.) Primary waves (P waves): P waves is sometimes referred to as longitudinal and compressional waves. They are also called primary waves because they spread more quickly than the other wave kinds across the medium. In P-waves, material particles oscillate in the direction of wave distribution by compression and expansion, precisely like a sound wave, around fixed points. The velocity of P-waves can be determined by the mathematical expression.

$$V_p = \sqrt{\frac{k+\frac{4\mu}{3}}{\rho}} \qquad 2.20$$

where (K) Bulk modulus, (μ) Shear modulus, and (ρ) density (Kearey *et al*., 2002; Lowrie, 2007; Reynolds, 2011).

2.) Secondary waves (S waves): Often they're called shear and/or transverse waves because they travel more slowly than P-waves across the medium. In S-waves, particles comprising the medium are driven in the direction perpendicular to the direction in which the wave travels. The medium is deformed along spherical surfaces in this case, as the wave radially propagates. The velocity of S-waves can be determined by the expression:

$$V_s = \sqrt{\frac{\mu}{\rho}} \qquad 2.21$$

where (μ) Shear modulus, and (ρ) density (Telford *et al*., 1990; Kearey *et al*., 2002; Lowrie, 2007; Reynolds, 2011).

Seismic surface waves do not penetrate deep into subsurface media of which two forms exist, Rayleigh waves and Love waves. (Telford *et al*., 1990; Kearey *et al*., 2002; Lowrie, 2007; Reynolds, 2011).

i) Rayleigh waves: They are called ground roll. They can be likened to waves on the water surface due to their ripple-like movement when travelling. Rayleigh waves will not be dispersive in a homogenous earth but in a double layer earth, when Rayleigh waves are 1 to 30 times the thickness of the top layer, they become dispersive. In general, longer wavelengths penetrate deeper and are more sensitive to deeper layers' elastic properties, while shorter wavelengths respond to the elastic properties of the shallow layers It is approximately 90 percent of the velocity of the S wave for a homogenous media, nevertheless they are much slower than body waves (Figure 2.4).

ii) Love waves: They are Horizontal polarized shear waves (SH waves) which exist only in the presence of a semi-infinite medium overlain by a finite upper layer of thickness.

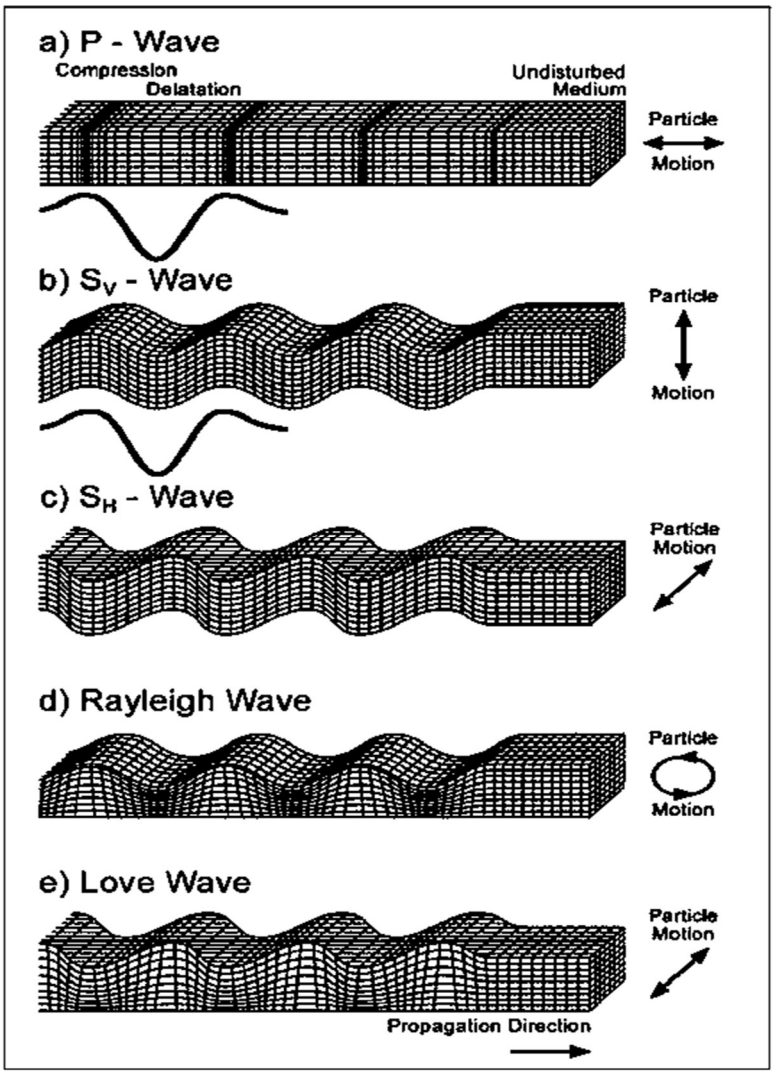

Figure 2.4: Propagation of seismic waves (After Lowrie, 2007)

Normally they go a little more rapidly than Rayleigh, around 90 percent of the S wave speed and also possess the highest amplitude (Figure 2.4).

Figure 2.5 depicts the propagation of waves in a medium. This is applicable also in seismic wave propagation through earth materials.

2.3.1 Refraction at a Horizontal Interface

The refraction method is illustrated for the case of the flat interface between two horizontal layers in (Figure 2.5). Let the depth to the interface be **(d)** and the seismic velocities of the upper and lower layers be **(V_1)** and **(V_2)** respectively **($V_1<V_2$)**. *The direct ray* from the shot point at **(S)** is recorded by a geophone **(G)** at distance **(x)** on the surface after time **(x/V_1)**. The travel-time curve for the direct ray is a straight line through the origin with slope **($m_1 = 1/V_1$).** The hyperbolic t–x curve for the *reflected ray* intersects the time axis at the two-way vertical reflection "echo" time **(t_0)**.

At great distances from the shot-point the reflection hyperbola is asymptotic to the straight line for the direct ray (Kearey *et al*., 2002; Lowrie, 2007; Reynolds, 2011).

The doubly refracted ray travels along the path **(SC)** with the velocity **(V_1)** of the upper layer, impinges with critical angle **(i_c)** on the interface at **(C)**, passes along the segment **(CD)** with velocity **(V_2)** of the lower layer, and returns to the surface along **(DG)** with velocity **(V_1)**. The segments **(SC)** and **(DG)** are equal, **($CD = x - 2SA$)** and the travel-time for the path **($SCDG$)** can be written:

$$t = \frac{2Sc}{V_1} + \frac{CD}{V_2} = \frac{2d}{V_1 \cos i_c} + \frac{x - 2d\tan_{\ c}}{V_2} \qquad 2.22$$

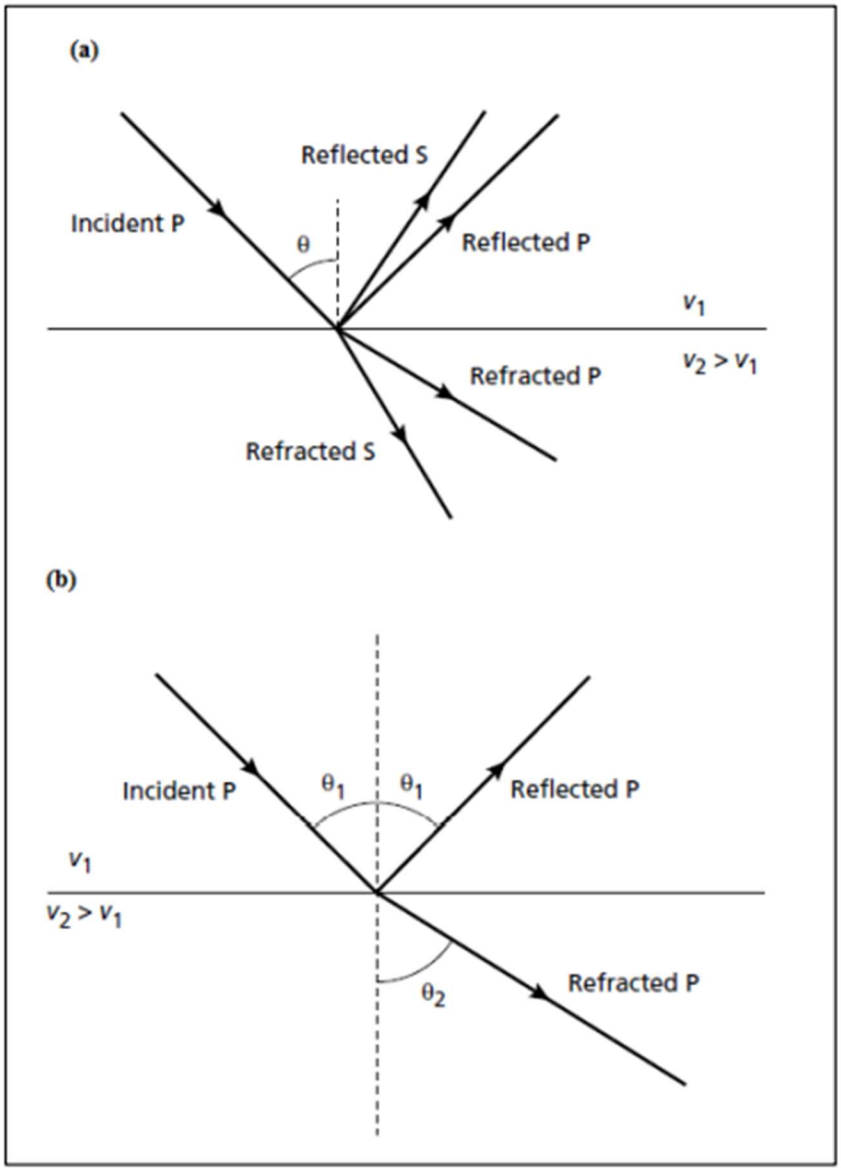

Figure 2.5: (a) Reflected and refracted P- and S-wave rays generated by a P-wave ray obliquely incident on an interface of acoustic impedance contrast, and (b) Reflected and refracted P-wave rays associated with a P-wave rays obliquely incident on an interface of acoustic impedance contrast (After Kearey *et al.,* 2002).

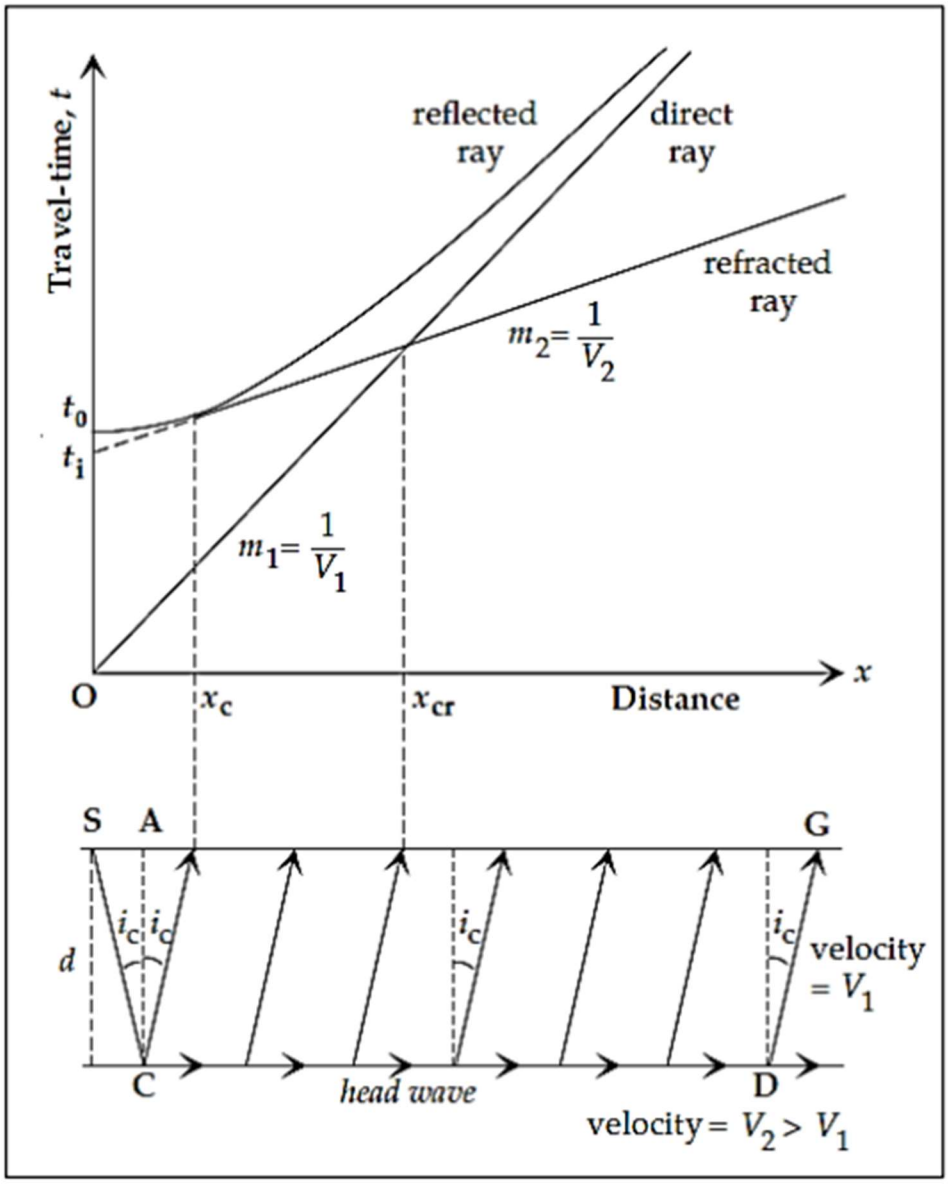

Figure 2.6: Travel-time versus distance curves for the direct ray and the reflected and refracted rays at a horizontal interface between two layers with seismic velocities V_1 and V_2 (After Kearey *et al.,* 2002).

Rearranging terms and using Snell's law (eq. 2.22), we get for the travel-time of the doubly refracted ray:

$$t = \frac{x}{V_2} + \frac{2d}{V_1} cosi_c \qquad 2.23$$

The doubly refracted rays are only recorded at distances greater than the critical distance **(x_c)**. The first arrival recorded at **(x_c)** can be regarded as both a doubly refracted ray and a reflection. The refraction t–x curve is found to intersect the time axis at *the intercept time* **(t_i)**, given by:

$$t_i = \frac{2d}{V_i} cosi_c = 2d \frac{\sqrt{V_2^2 - V_1^2}}{V_1 \cdot V_2} \qquad 2.24$$

Close to the shot-point the direct ray is the first to be recorded. However, the doubly refracted ray travels part of its path at the faster velocity of the lower layer, so that it eventually overtakes the direct ray and becomes the first arrival. The straight lines for the direct and doubly refracted rays cross each other at this distance, which is accordingly called the *crossover distance*, **(x_{cr})**:

$$x_{cr} = 2d \cdot \sqrt{\frac{V_2 + V_1}{V_2 - V_1}} \qquad 2.25$$

Tables of seismic velocities of different earth materials given by Kearey *et al.,* (2002) and McDowell *et al.,* (2002) are presented in Tables 2.1 and 2.2

2.3.2 Limitations of Seismic Refraction Method

i. The existence of certain beds or layers with insufficient velocity contrast or thickness cannot be detected by the refraction method. These layers called hidden layers or blind zones.

ii. Seismic refraction observations require relatively large source-receiver offsets (distances between the source and where the ground motion is recorded, the receiver).

Table 2.1: Compressional wave velocities (Vp) in earth materials (Kearey *et al*., 2002).

	v_p (kms^{-1})		v_p (kms^{-1})
Unconsolidated materials		**Metamorphic/igneous rocks**	
Sand (dry)	0.2–1.0	Granite	5.5–6.0
Sand (water-saturated)	1.5–2.0	Gabbro	6.5–7.0
Clay	1.0–2.5	Ultramafic rocks	7.5–8.5
Glacial till (water-saturated)	1.5–2.5	Serpentinite	5.5–6.5
Permafrost	3.5–4.0	**Pore fluids**	
Sedimentary rocks		Air	0.3
Sandstones	2.0–6.0	Water	1.4–1.5
Tertiary sandstone	2.0–2.5	Ice	3.4
Pennant sandstone (Carboniferous)	4.0–4.5	Petroleum	1.3–1.4
Cambrian quartzite	5.5–6.0	**Other materials**	
Limestones	2.0–6.0	Steel	6.1
Cretaceous chalk	2.0–2.5	Iron	5.8
Jurassic oolites and bioclastic limestones	3.0–4.0	Aluminium	6.6
Carboniferous limestone	5.0–5.5	Concrete	3.6
Dolomites	2.5–6.5		
Salt	4.5–5.0		
Anhydrite	4.5–6.5		
Gypsum	2.0–3.5		
Shale	1.8–4.9		

Table 2.2: Shear waves velocity of some earth materials (McDowell *et al.,* 2002).

Materials	Vs (m/s)
Air	0
Water	0
Sands and clays	100-500
Glacial till	600 – 1300
Chalk	600 – 1500
Strong limestone	1500 – 3500
Weathered granite	500 – 1500
Fresh granite	1500 – 3000
Slate	2500 – 3800

iii. Seismic refraction only works if the speed at which motions propagate through the Earth increases with depth.

iv. Seismic refraction observations are generally interpreted in terms of layers. These layers can have dip and topography.

v. Seismic refraction observations only use the arrival time of the initial ground motion at different distances from the source (i.e., offsets).

2.3.3 Field Operation

A number of different of noises may contaminate our seismic measurements (Kearey *et al.,* 2002). Since we control the source of the seismic energy, we can control some types of noise, but not all of it. Seismic noises could be either:

1. **Uncontrolled Ground Motion:** Anything that causes the ground to move, other than your source, will generate noise. Such as; wind, traffic, people walking, moving animals, etc.
2. **Electronic Noise:** Geophones transform the ground motion they detect into electrical signals. These signals are then conveyed down the cable, magnified and registered by the recording system. Therefore, anything that can cause electrical signal shifts generates noise in our recorded data. For example, loose connections between the geophones and the cable or cable and the recording system.
3. **Geological Noise:** We can take into account any type of subsurface geological structure that we cannot easily interpret as a source of noise.

CHAPTER THREE

MATERIALS AND METHODS OF STUDY

The methods adopted in this study were lithologic logging, seismic refraction and multichannel analysis of surface waves (MASW), 2D electrical resistivity tomography and the vertical electrical sounding (VES) of the electrical resistivity method. The methods were used because of their ability to delineate the extent of sub-soil variation in both laterally and vertically in depth based on sub-soil physical properties. The data acquisition map is shown in Figure 3.1.

3.1 Electrical Resistivity Instrumentation

The field materials used are:

i. SuperSting R8 & R1 earth resistivity meter.
ii. Electrodes
iii. Cable
iv. Hammer
v. Meter Rule
vi. Battery
vii. GPS

The electrical resistivity method employed the 2-D Electrical Resistivity Tomography and the Vertical Electrical Sounding (VES). The SuperSting R8 was used for the acquisition of the 2D electrical resistivity tomography data (Figure 3.2). The SuperSting R8 system consists of a resistivity/IP meter, 112 electrodes that are connected via cable, and an energy source (battery) that is used to power a resistivity/IP meter. Data was acquired for six traverses using the Dipole – Dipole array. The distance between each traverse is about 60 meters and has a spread length of 224 meters.

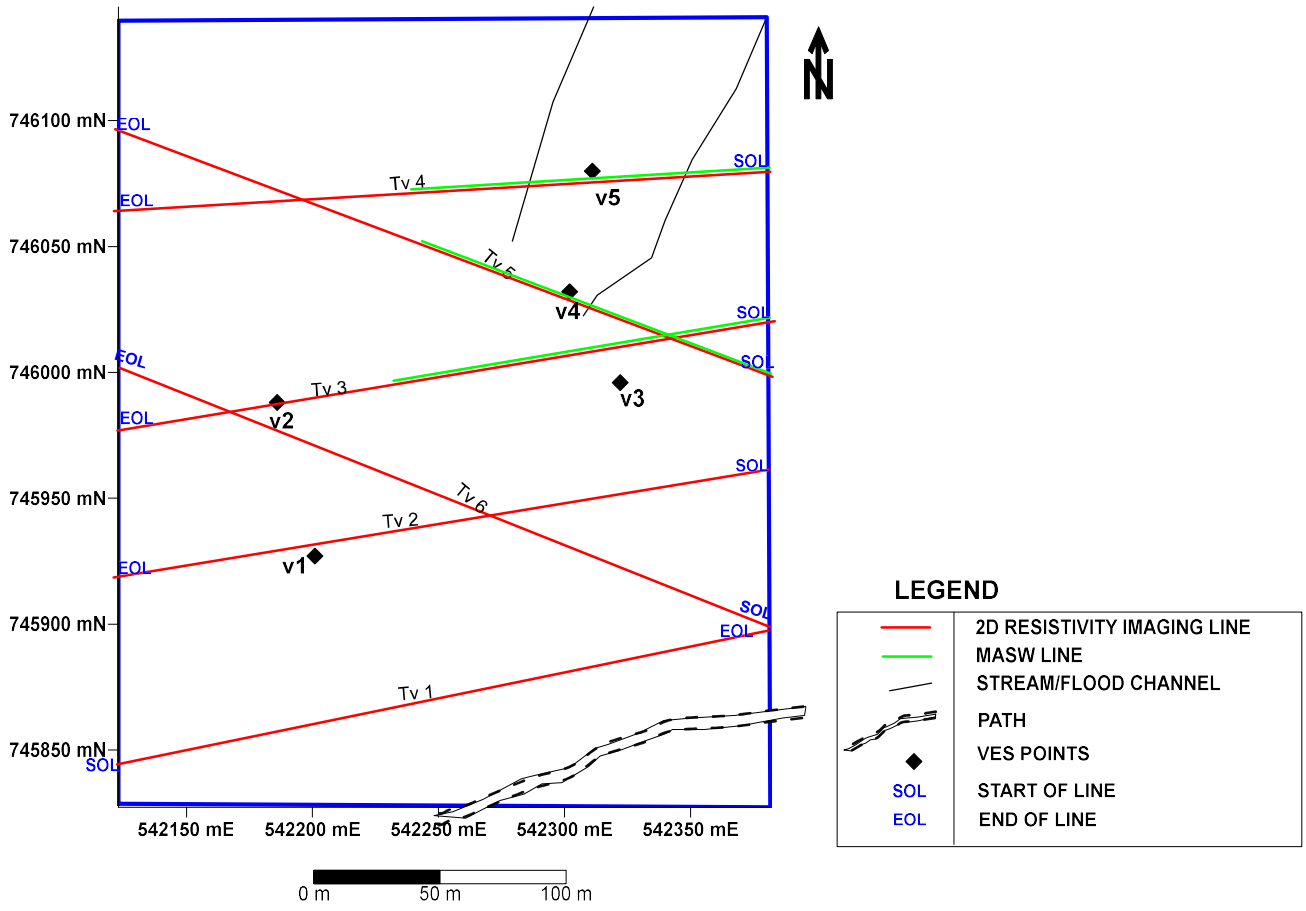

Figure 3.1: Data Acquisition Map of the Study Area

Figure 3.2: Field setup for SuperSting R8 Earth Resistivity Meter

The SuperSting R1 was applied for the acquisition of the Vertical Electrical Sounding (VES) data using Schlumberger array configuration. The resistance and the apparent resistivity of the soil at each point were recorded.

3.2 2D Seismic Refraction Tomography and MASW Instrumentation

The field materials used are:

i. Terraloc Pro Seismograph.

ii. 48 geophones with a frequency of 4.5Hz.

iii. Geophone cables

iv. Shot cable and shot geophone

v. Batteries.

vi. Global Positioning System (GPS).

vii. Measuring Tape

viii. Sledge Hammer weighing 5 kg.

ix. Base plate.

Forty-eight (48) geophones were mounted on the ground and connected to two seismic ground cables with a total of 48 outlets. These seismic geophone cables are used to send the electrical pulse from each geophone to the seismograph to record the seismic signals. The seismic source was generated by hitting a 5 kg sledge hammer on a rubber plate. During the survey, two offset shots and three split shots were fired.

Terraloc Pro seismograph was used during the data acquisition (Figure 3.3). The sampling rate used in the course of the survey is 100 μs and the window time length is 204.8 ms, the reason for the use of the Terraloc Pro seismograph is because of its wide range of sampling rates.

Figure 3.3: Field setup for ABEM Terraloc Pro Seismograph

After the equipment has been set up, the noise level was monitored on the seismograph. The lowest acceptable noise level was determined before shots were fired.

The only difference in the data acquisition procedure between the 2D seismic refraction tomography and 2D Multichannel Analysis of Surface Waves (MASW) is the way their data is being acquired, unlike the conventional 2D refraction tomography where the geophones are planted on the ground and the specified kind of shot type either two offset shot, three split shot, for this study two offset shot and three split shot. End-on shot is acquired only at the offset of the spread, preceding this is the removal of the first geophone from it initial position and positioning it at the end of the spread, making it the last geophone and moving the geophone cable towards the new last geophone, known to the first geophone this process is called roll along.

3.3 Data Processing

3.3.1 Electrical Resistivity Tomography (ERT)

For inversion of the 2-D resistivity data, Advance Geophysical Incorporated (AGI) EarthImager software was used. This software generates an apparent resistivity inverted section from the measured field data, by comparing the measured model with a computed theoretical model. A final inverted model of apparent resistivities, which is taken to be the sub-surface model, is then generated.

3.3.2 Vertical Electrical Sounding (VES)

The technique profiles the subsurface layering by their differing apparent resistivity values. Depth sounding type curves include the H, K, A and Q type curves. VES are usually interpreted using the subjective interpretation approaching known as the partial curve matching (Bhattacharya and

Patra, 1968). The VES data were drawn on a transparent surface in order to do this. The technique of partial curve matching included the use of standard two (2) master layer and four (4) auxiliary curves (H, K, A and Q). This approach selects matches the curve segment-by-segment. In order to limit the interpretation of the computer employing iteration software, WINRESIST the results of VES curves obtained from a partial curve matching are now used. This sometimes decreases the depth estimated. The results of the software iteration illustrate the semi-quantitative/quantitative analysis to appreciate the resistivity, thickness and depth. The vertical electric sounding results (VES), obtained using the WINRESIST program, are shown as depth sounding curve. The apparent readings for resistivity against electrode separation on a log-log paper are plotted, which was matched with the curve. Based on the results of the interpreted VES data, geoelectric sections were developed. See in Appendix A

3.3.3 Seismic Refraction Tomography Data Processing

The speed of sounds through the surface varies depending on the structure of the material and its compaction. Seismic energy transmitted from the source on the surface is refracted at the limits between various media and returns to the surface in due course. Seismic refraction surveys use this phenomenon to characterize the soil structure by looking at the time required to convey energy through the subsurface (Reynolds, 2011).

The seismic refraction survey method uses seismic energy that returns to the surface after traveling through the ground along refracted ray pathways. Unlike the seismic reflection method, only a few processing steps will be used in the refracted method to improve data and significantly reduce noise.

3.3.3.1 DC Offset Removal

This process is the first stage of data the processing data once the data has been acquired by the seismograph. DC offset noise (also called DC bias, DC component, or DC coefficient) is a 0 Hz frequency component which distort the data. Being a low frequency noise, it is often eliminated using a Butterworth high-pass filter. In this research, the software used for this processing is the "Reflex2DQuick" software.

3.3.3.2 Geometry Assignment and Editing

The geometry of the field is written to the data (trace headers) in order to associate each trace with its respective shot, offset, channel, and common midpoint (CMP). This is done by providing the longitude, latitude, and elevation of each shot point and geophone using the GPS. After DC offset removal and geometry assignment, we can modify the seismic data to mute the wrong traces (noise channels, poorly planted geophones etc.) or rectify the polarity problems.

3.3.3.3 Frequency Filtering

Frequency filters differentiate between selected waveform input frequency components and noise. Frequency filters are used when the signal and noise components of the waveform have different frequency qualities and can therefore be separated on this basis (Oz Yilmaz, 2001). The main types of filtering are:

1. high-pass filter: also referred to as a low-cut filter, is a filter that transmits high-frequency signals but attenuates signals with frequencies below the cut-off frequency.
2. a low-pass filter: also referred to as a high-cut filter, is a filter that transmits low-frequency signals but attenuates signals with frequencies higher than the cut-off frequency.

3. band-pass filter: is a filter that passes signals only in a definite frequency band while attenuating all signals outside this band.

3.3.3.4 Picking of the First Arrivals and Generating the Travel Time curves

When performing a refraction survey, the time of arrival of the first wave is the only information extracted from the recorded seismograms that is used. It may be difficult picking the first arrivals at remote geophones where the signal-to-noise ratio is low. Some of the later peaks and troughs in the same wave train are likely to be stronger, and sometimes it is possible to work back from them to estimate the position of the first break. Picking the first arrivals was done using a software called "SeisImager" that is aided by a tool called "Pickwin".

The data extracted from the refraction survey consists of sets of first-arrival times measured at geophones at different distances from the source position. Since these are graphed against vertical time axes and horizontal distance axes (a diagram called travel time curve or time-distance curve), the slope of any line is equal to the reciprocal of a velocity, i.e., steep slopes correlate to slow velocities, while the gentle slope correlates to high velocities.

3.3.3.5 Velocity modelling

The interpretation of the seismic refraction data is based on the modeling and inversion of the acquired seismic velocity. The velocities are determined by the travel time plot for each seismic line. By simulating the paths taken through the subsurface by seismic energy or 'ray tracing,' the thickness and extension of each layer in the model can be adjusted in an iterative manner until a solution is reached. This produces a cross-section velocity model of the subsurface. Borehole records can further calibrate the data to provide subsurface layer levels across the survey line.

There are many techniques used for seismic refraction inversion, one of which is known as the ***Tomographic Method*** that is used during this research. The tomographic method involves the production of an initial velocity model, and then iteratively tracing the rays through all of the model, comparing the calculated travel times with the measured travel times, improving the model and repeating the process until the difference between the calculated and the measured time is reduced.

The initial velocity model is developed utilizing ***time-term technique,*** which is the Least-Squares linear approach, to determine the best discrete-layer solution for the data. The tomographic method provides more realistic profiles where there are gradational vertical changes in velocity (e.g. soil gradation into saprolite and then rock gradation) or lateral changes in velocity (e.g., fracture zones, vertical contacts, or solution cavities in rock).

The inversion was done using SeisImager, which again is facilitated by a tool called Plotrefa. The horizontal axis represents the long-profile distance in meter, while the vertical axis represents the elevation in meter. Color contours are a tomographic model where the subsurface is regarded as a layer of discrete blocks and the best-fit velocity value for each block is calculated.

3.3.4 MASW Method

The Multichannel Surface Wave Analysis (MASW) method is a geophysical method for generating the shear-wave velocity (Vs) profile (i.e., Vs versus depth) by analyzing Rayleigh-type surface waves on a multichannel record to evaluate the elastic characteristic (stiffness) of the ground. (Taipodia and Dey, 2012).

MASW first of all measures the seismic surface waves actually generated from the seismic sources, analyzes the velocity distribution of those surface waves, and finally derive the shear wave velocity (Vs) variations below the surveyed area which are most important in the understanding of

the propagation velocity trend of the surface waves. The shear wave velocity is linked to the stiffness of the medium through which the waves travel. Surface wave surveying is therefore a useful tool for determining variation in ground stiffness with depth. Comparison to standard seismic survey methods, such as cross-hole and downhole, the MASW is cost-effective and saves time (Reynolds, 2011; Taipodia and Dey, 2012).

Regarding the way surface waves are produced, there are two main types of waves. (Taipodia and Dey, 2012):

1. passive MASW: Where surface waves are formed by natural sources extraneous to the survey, such as traffic and tidal movements.
2. active MASW: Where surface waves are created by a source of impact, such as a sledge hammer or a weight drop.

The active MASW method was used in this study, where the seismic source was a sledge hammer, and 48-geophones, which were arranged in a linear array and connected to a multi-channel seismograph, acquiring data concurrently in all geophones. The entire MASW procedure consists of three steps:

1. Collecting multi-channel field records.

2. Extract the dispersion curves.

3. Invert this dispersion curve to obtain a Vs (Shear wave velocity) profile.

The 2D Vs model was developed by incorporating a range of 1D Vs models together. This technique was used at three traverses along lines 3, 4 and 5 respectively. In order to produce a 2D Vs profile, a new acquisition was made with vertical low-frequency geophones (e.g., 4.5 Hz) that are sensitive to surface waves. The source used was a sledge hammer and the geophone interval was 2 m for 48 geophones. The overall length of the profile is 143 m. However, during the survey, 48 offset points were acquired where the range of the shot point range was between 1 and 2 m.

3.4 Computation of Engineering Parameters from Seismic Compressional and Shear Waves

Bulk Density (ρ), Compressibility (β), Bulk Modulus (K), Dynamic Shear Modulus (G) and Rock mass Quality (Q) were derived from the Compressional Wave Velocity (Vp) and Shear Wave Velocity (Vs). Presented below are the equations that relate these quantities with seismic velocities.

Bulk Density (ρ): According to Gardner *et al.,* (1974), bulk density of earth materials is given as

$$\rho = aV_p^{0.25} \tag{3.1}$$

where ρ is bulk density (g/cc), V_p is compressional seismic wave velocity (m/s) and a is a constant which is = 0.31

Shear modulus (G) is given as

$$V_s = \sqrt{\frac{G}{\rho}} \tag{3.2}$$

where V_s is shear wave velocity (m/s), G is Shear Modulus (Pa) and ρ is bulk density (g/cc)

Bulk modulus (K) is given as:

$$V_p = \sqrt{\frac{K+\frac{4}{3}G}{\rho}} \tag{3.3}$$

Compressibility (β) is given as

$$\beta = \rho(V_p^2 - \frac{4}{3}V_s^2)^{-1} \tag{3.4}$$

where ρ is bulk density (g/cc), V_p compressional seismic wave velocity (m/s) and V_s is shear wave velocity (m/s).

Rock-mass Quality (Q) is given as

$$Log\ (Q) = V_p - 3.5\ km/s \tag{3.5}$$

CHAPTER FOUR

RESULTS AND DISCUSSION

4.1 The Vertical Electrical Sounding (VES) Results

Presented in this section are the VES sounding curves (Figure 4.1). For all the points investigated, the VES curve type obtained is the "HK" type curve. This indicated that four (4) geoelectric layers were delineated. The geoelectric layers delineated were interpreted to correspond in their order of succession from the ground surface to a silty clay/clayey topsoil, a low resistivity clay layer, a clayey sand layer and the fourth geoelectric layer of low resistivity suspected to be clay.

Topsoil resistivities and thickness varied from 12 to 51 ohm-m and 0.4 to 0.8 m respectively. The second layer which was interpreted as low resistivity clay has resistivities and thicknesses ranging from 3 to 7 ohm-m and 1.5 to 5.2 m respectively. The third layer which was interpreted as clayey sand has resistivities and thicknesses varying between 13 and 163 ohm-m, and 1.6 and 9.1 m respectively. The resistivity of the fourth geoelectric layer (which is also a low resistivity clay) varied between 3 to 46 ohm-m. The depth to the fourth layer ranged from 5.7 to 14.6 m. The summary of the geoelectric parameters were presented in Table 4.1.

4.1.1 The Proximal Lithological Logs

To validate the VES modelling and interpretation, the VES results were compared with the lithologic log obtained at Borehole Point 1(Bh-1) and Borehole Point 2 (Bh-2) which were located at distances 293 m and 280 m respectively from the southernmost end of the study area. The lithologic logs delineated five (5) geologic sequences which were the soft/firm stiff clay with an average thickness of 3 m, medium to coarse grained sand having an average thickness of 6 m, inorganic/silty clay having an average thickness of about 3 m, firm dark organic clay having

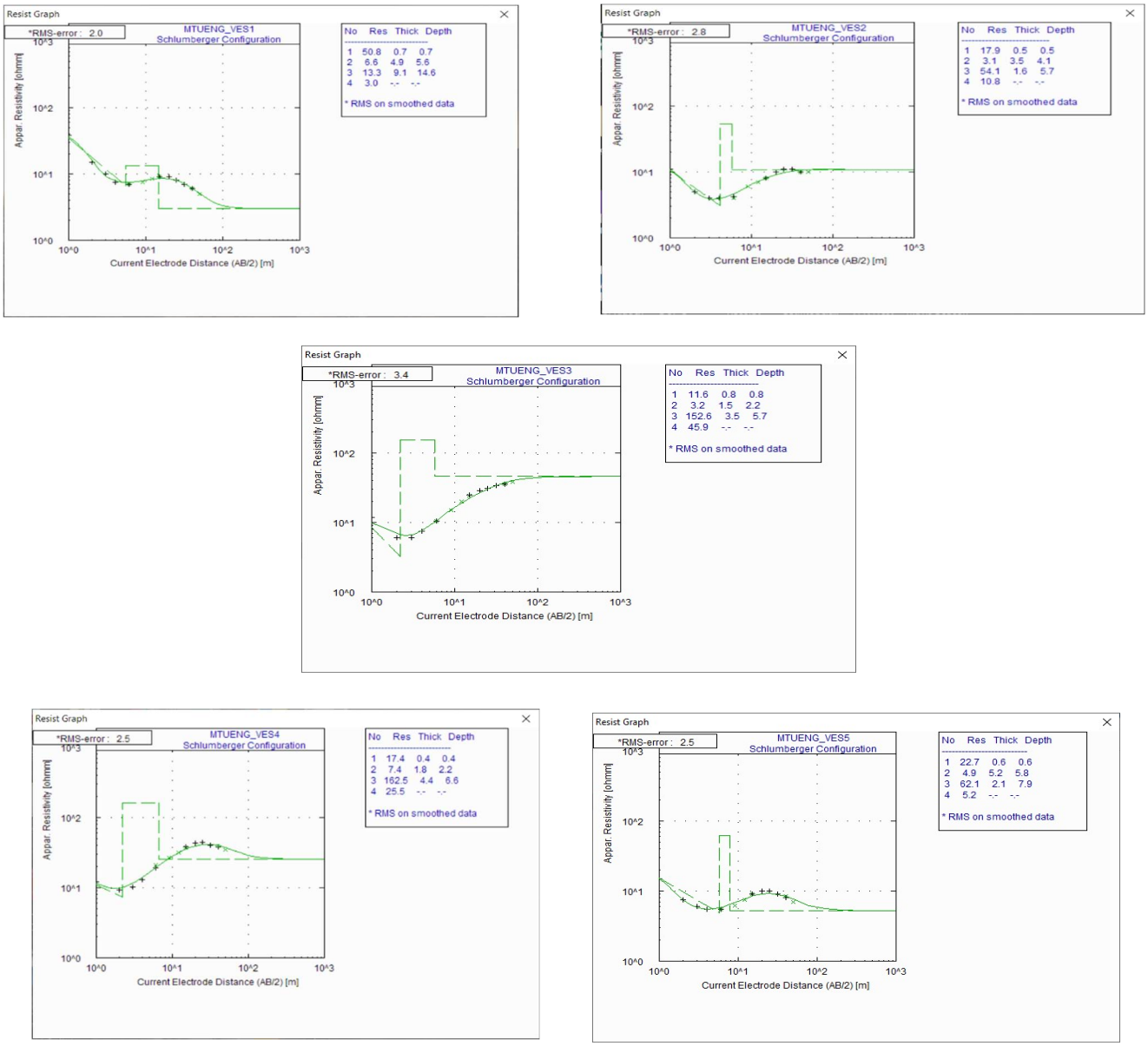

Figure 4.1: VES curves for VES 1 (top left), VES 2 (top right), VES 3 (centre), VES 4 (bottom left) and VES 5 (bottom right).

Table 4.1: VES Interpretation Results

VES No	Coordinates		Layer No	Resistivity (Ωm)	Thickness (m)	Depth (m)	Lithology	VES Type Curve
	Easting	Northing						
1	542201 mE	745927 mN	1	51	0.7	0.7	Topsoil	HK
			2	7	4.9	5.6	Clay	
			3	13	9.1	14.7	Clayey Sand	
			4	3	-	-	Clay	
2	542186 mE	745988 mN	1	18	0.5	0.5	Topsoil	HK
			2	3	3.5	4.0	Clay	
			3	54	1.6	5.6	Clayey Sand	
			4	11	-	-	Clay	
3	542322 mE	745996 mN	1	12	0.8	0.8	Topsoil	HK
			2	3	1.5	2.3	Clay	
			3	153	3.5	5.8	Clayey Sand	
			4	46	-	-	Clay	
4	542302 mE	746032 mN	1	17	0.4	0.4	Topsoil	HK
			2	7	1.8	2.2	Clay	
			3	163	4.4	6.6	Clayey Sand	
			4	26	-	-	Clay	
5	542311 mE	746080 mN	1	23	0.6	0.6	Topsoil	HK
			2	5	5.2	5.8	Clay	
			3	62	2.1	7.9	Clayey Sand	
			4	5	-	-	Clay	

thicknesses between 13.0 m and 16.5 m, and silty clay/silty sandy clay whose whole extent was not penetrated (Figures 4.2(a) and (b)).

As presented in Section 4.1, the VES probed generally less than 20 m (maximum AB/2 being 40 m) and delineated just four geoelectric sequence which were the silty clay/clayey topsoil, a low resistivity clay layer, a clayey sand layer and the fourth geoelectric layer of low resistivity suspected to be clay. When compared, both the lithologic log (Bh-2) and VES model (VES 1 which is closest to Bh-2) were essentially the same only that the:

i. topsoil was not discriminated on the borehole log
ii. inorganic/silty clay (third layer on the lithologic logs) was not resolved by the VES (due to the problem of suppression associated with conductive thin beds)
iii. the sand layer interpreted as clayey sand on the VES model together with the clay layer overlying it may have likely been overestimated (Figure 4.3) though not certainly.

4.2 The Geoelectric Sections

Geoelectric sections were generated for the purpose of layer and layer thickness correlation across proximal VES points. Based on the distribution of the VES points (Figure 3.1), VES 1 and VES 2; VES 3, VES 4 and VES 5; VES 1 and VES 3; as well as VES 2 and VES 4 were used to generate the geoelectric sections presented in Figures 4.4 (a), (b), (c) and (d) respectively. From the geoelectric sections, it can be inferred that:

i. the clayey sand layer which is the relatively more competent layer thins northward for most part of the study area (Figures 4.4 (a), (b) and (c)) except in a portion of the western part where this layer is relatively thinner in the southern region (Figure 4.2 (d)).

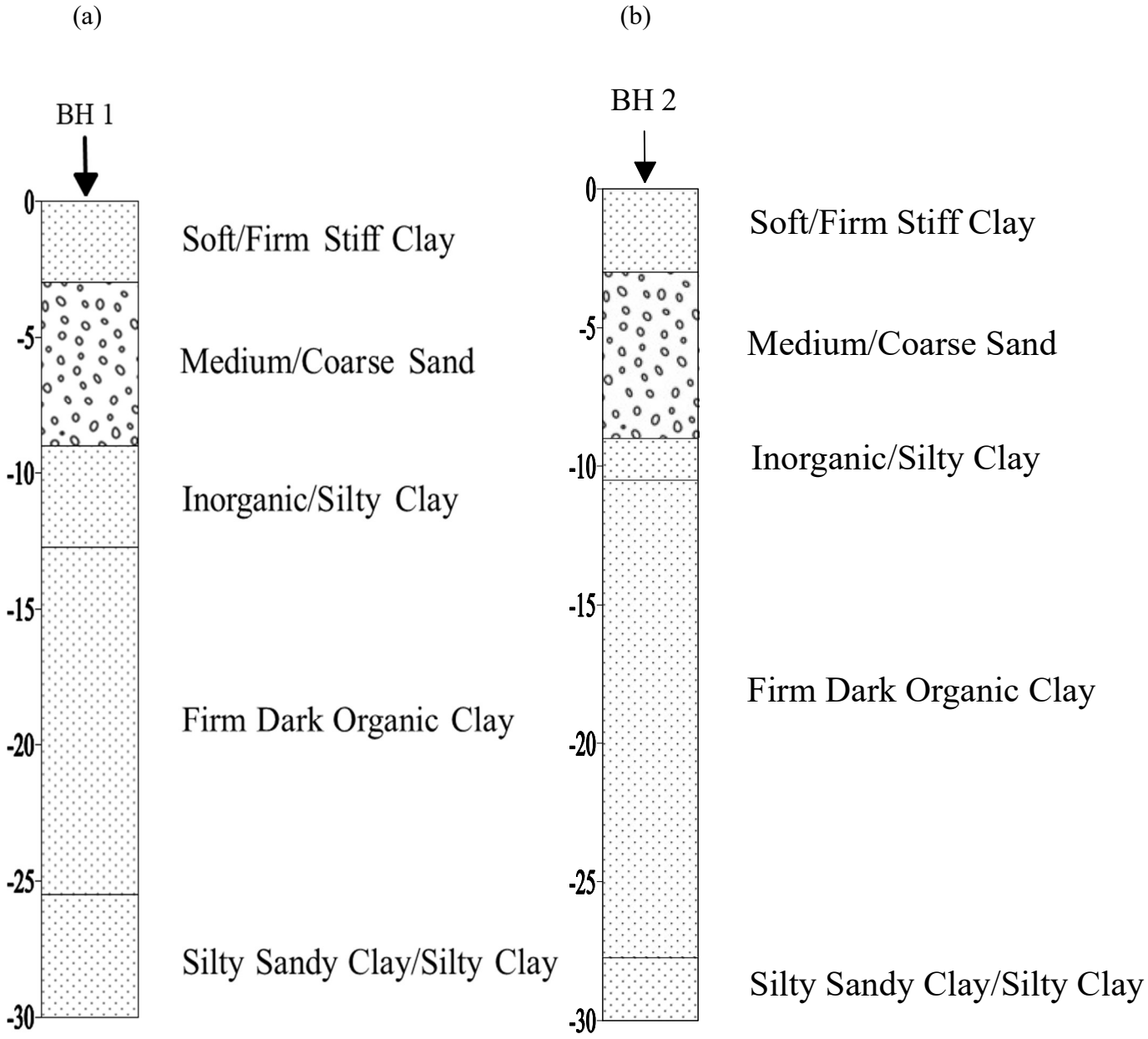

Figure 4.2 (a) and (b): The Lithologic Logs at Borehole Points 1 and 2.

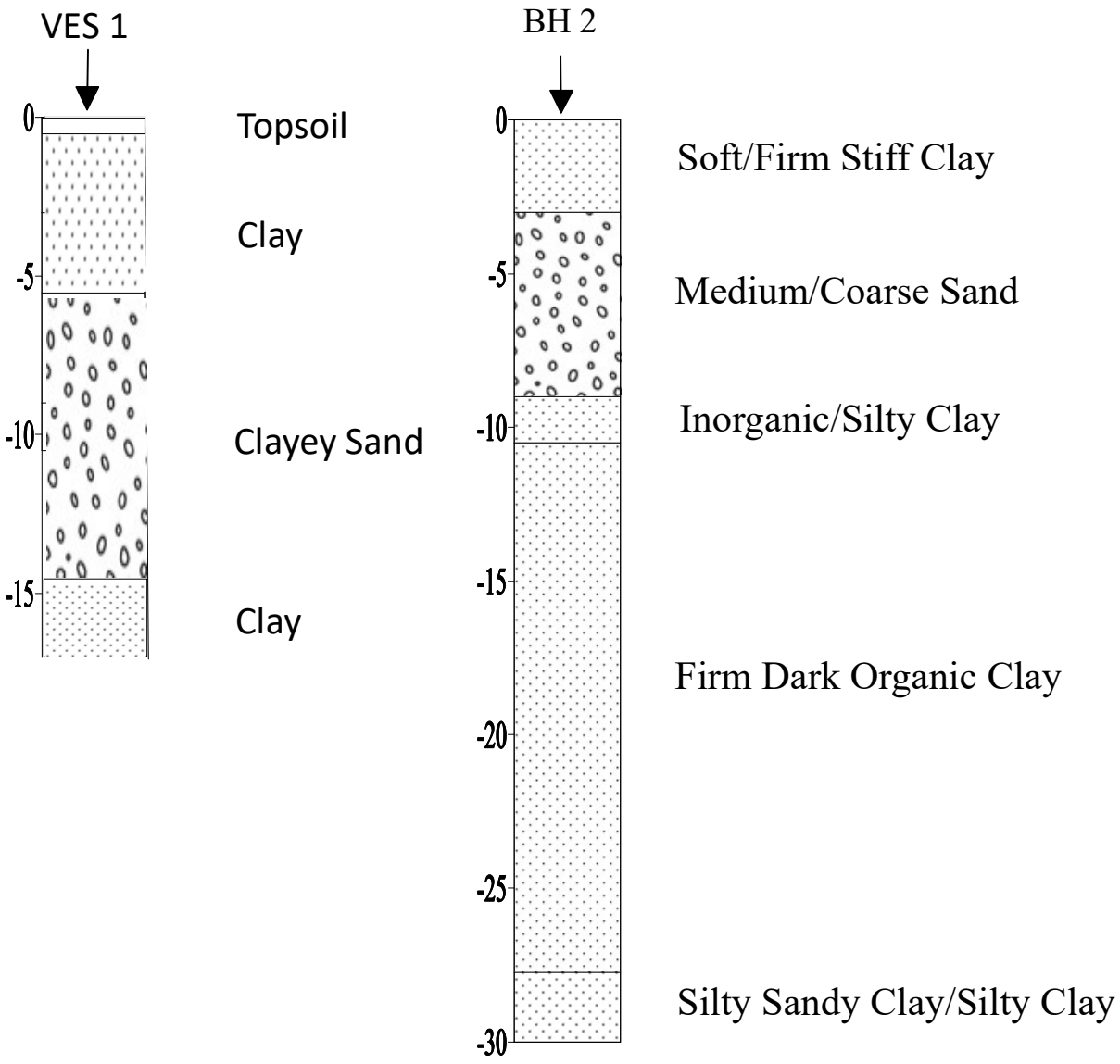

Figure 4.3: Comparison of the VES model (VES 1) and the lithologic log (Borehole 2)

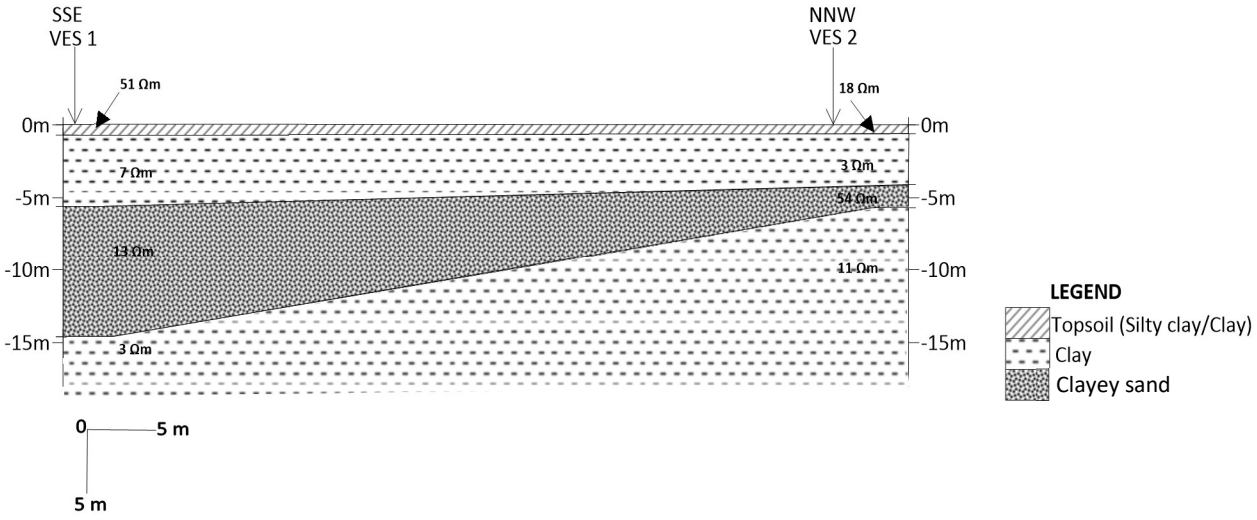

Figure 4.4 (a): Geoelectric Section connecting VES 1 and VES 2

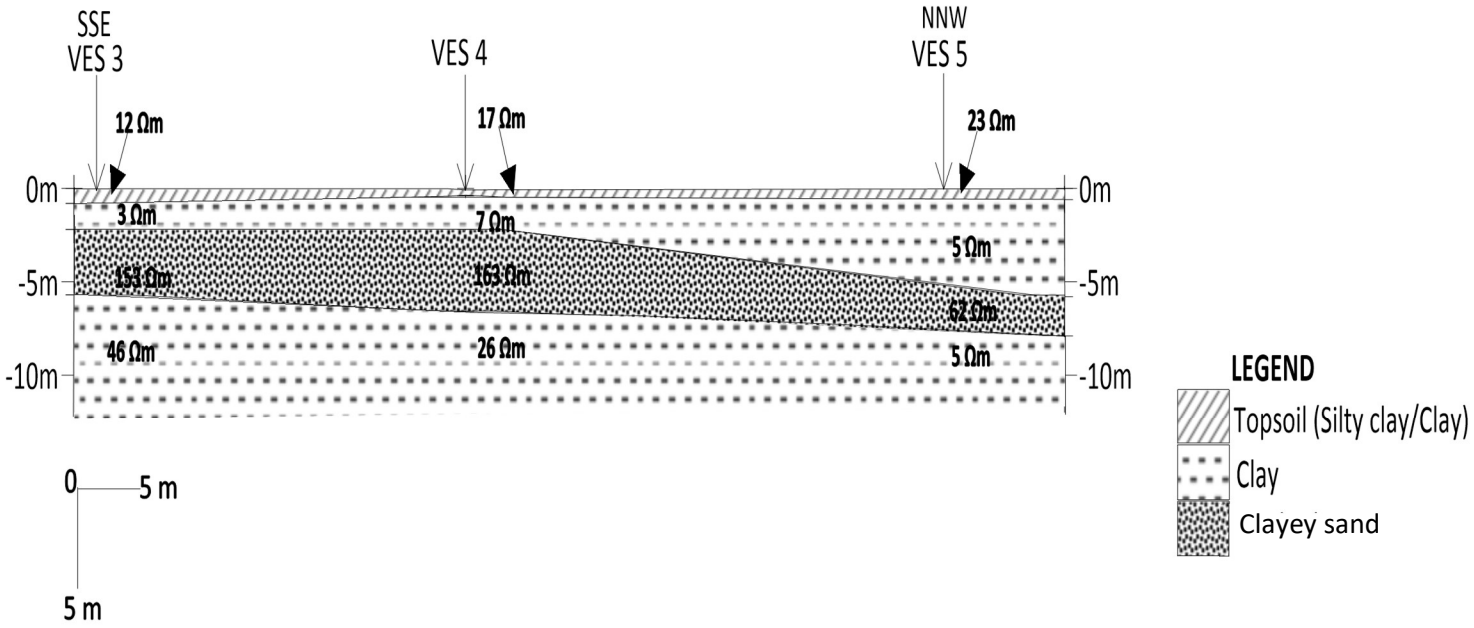

Figure 4.4 (b): Geoelectric Section connecting VES 3, VES 4 and VES 5

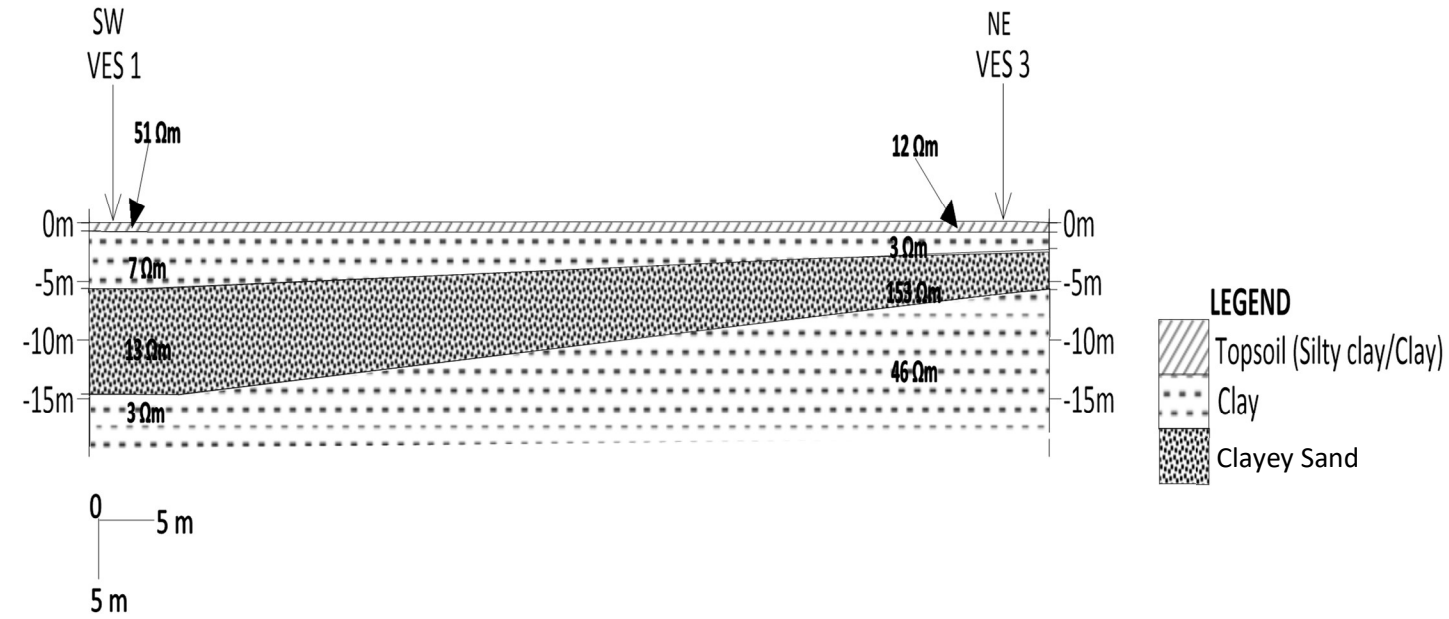

Figure 4.4 (c): Geoelectric Section connecting VES 2 and VES 4.

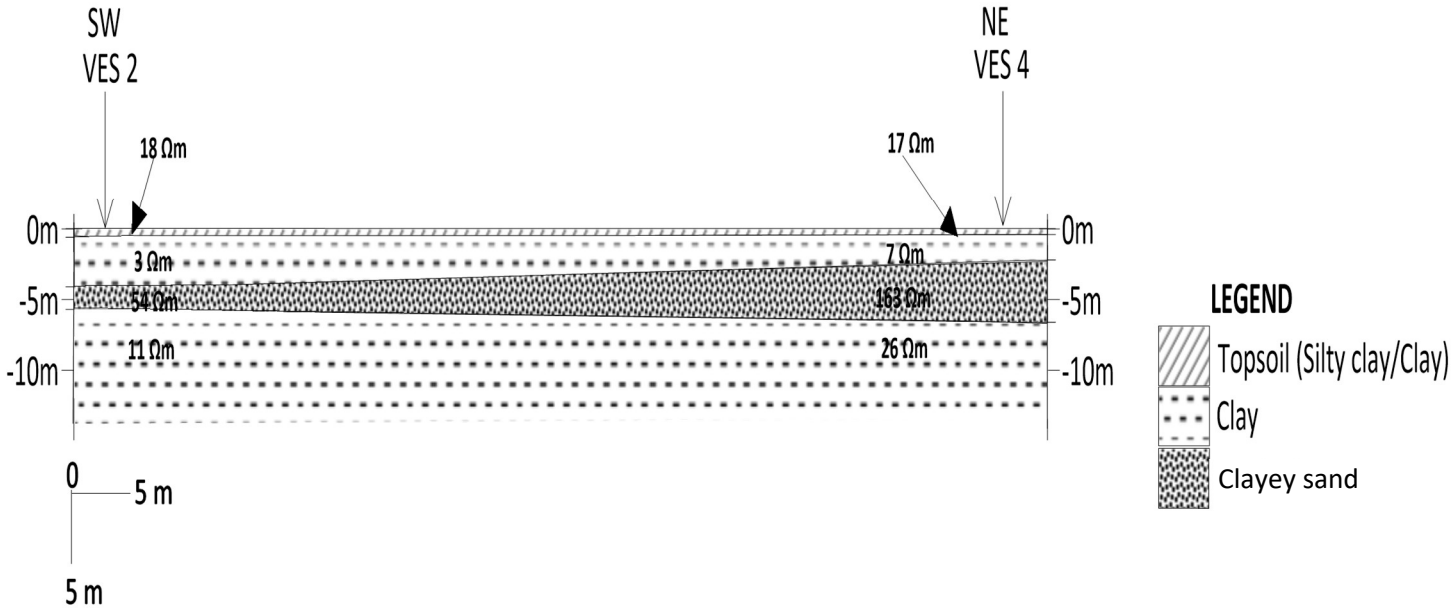

Figure 4.4 (d): Geoelectric Section connecting VES 1 and VES 3.

ii. depth to the clayey sand layer ranges from 2.2 to 5.8 m. This invariably means that to a good approximation the upper 2.2 to 5.8 m of earth material in the study area are constituted of incompetent clayey material.

4.3 The 2D Electrical Resistivity Inverted sections

Six (6) 2D electrical resistivity inverted sections of the subsurface were generated along Traverses 1, 2, 3, 4, 5 and 6. The relative positions of the traverses to one another is shown in Figure 3.1. Generally, between three (3) to four (4) geoelectric layers were delineated across all the sections. These layers are a low resistivity top soil, a relatively high resistivity layer, another low resistivity layer and another relatively higher resistivity layer (figures 4.5 (a), (b), (c), (d), (e) and (f)).

4.3.1 Traverse 1 (Figure 4.5 (a))

This is the southernmost traverse. It trends in the ENE-WSW direction (Figure 3.1). The top soil resistivity and thickness varied between 2 and 22 ohm-m, and about 1.5 to 6.2 m respectively while the resistivity and thickness of the second layer (having relatively high resistivity) varied between 29 to 135 ohm-m, and about 6 to 12 m respectively. The third layer which is another low resistivity layer has resistivity ranging from 2 to 29 ohm-m and thickness ranging from about 25 m (at the eastern end) to over 30 m at the western end. The fourth layer was only delineated at the eastern region of the traverse. It has a relatively higher resistivity (between 17 and 29 ohm-m) than the overlying layer. The end of this layer was not imaged by the inverted section. The total depth imaged by the 2D inverted section is 49.7 m. The third layer, which is likely clayey, is the thickest layer delineated in the inverted section.

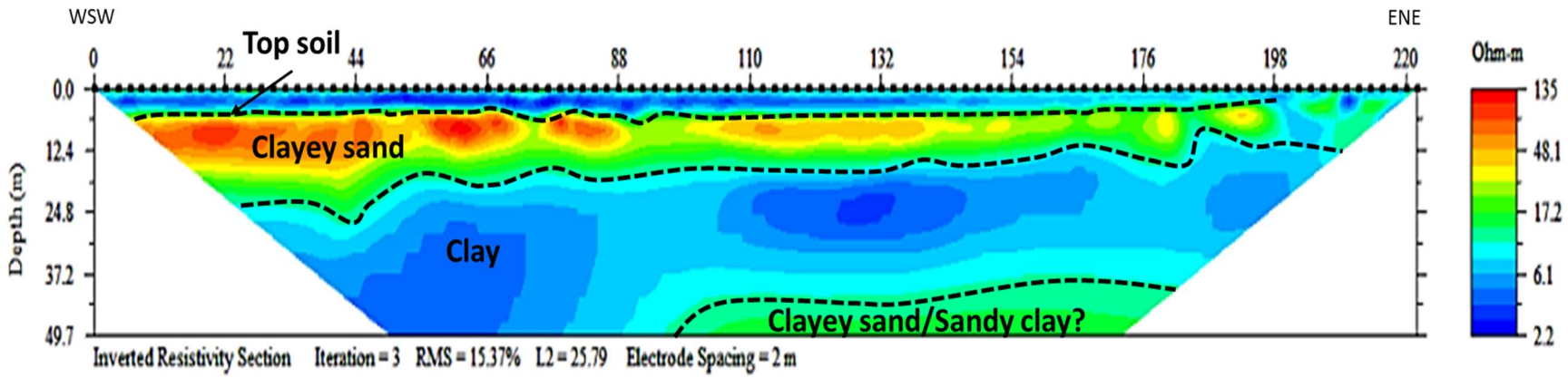

Figure 4.5(a): 2D Electrical Resistivity Inverted section along Profile 1

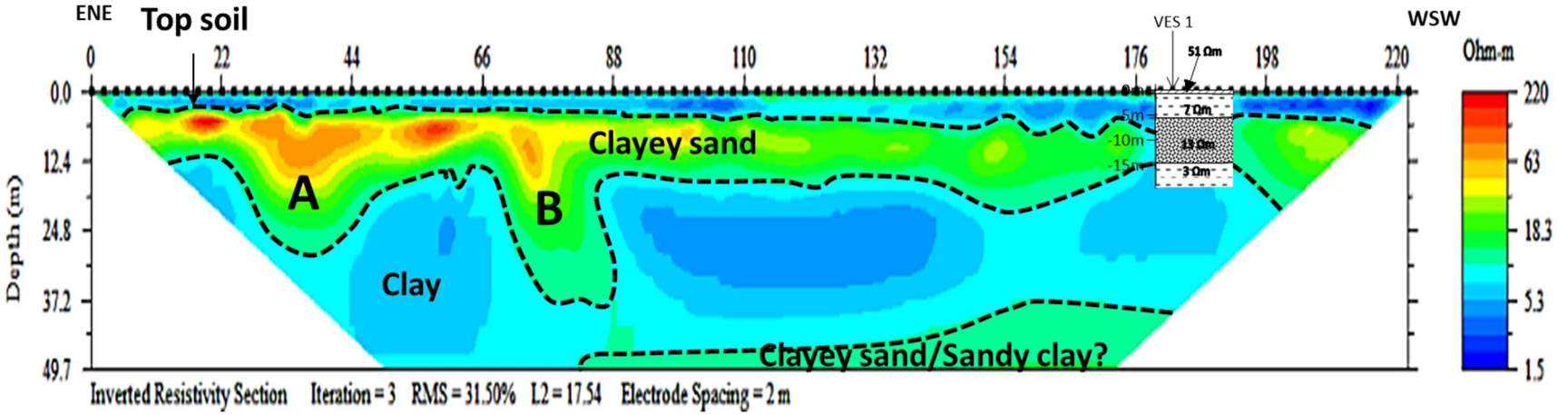

Figure 4.5(b): 2D Electrical Resistivity Inverted section along Profile 2

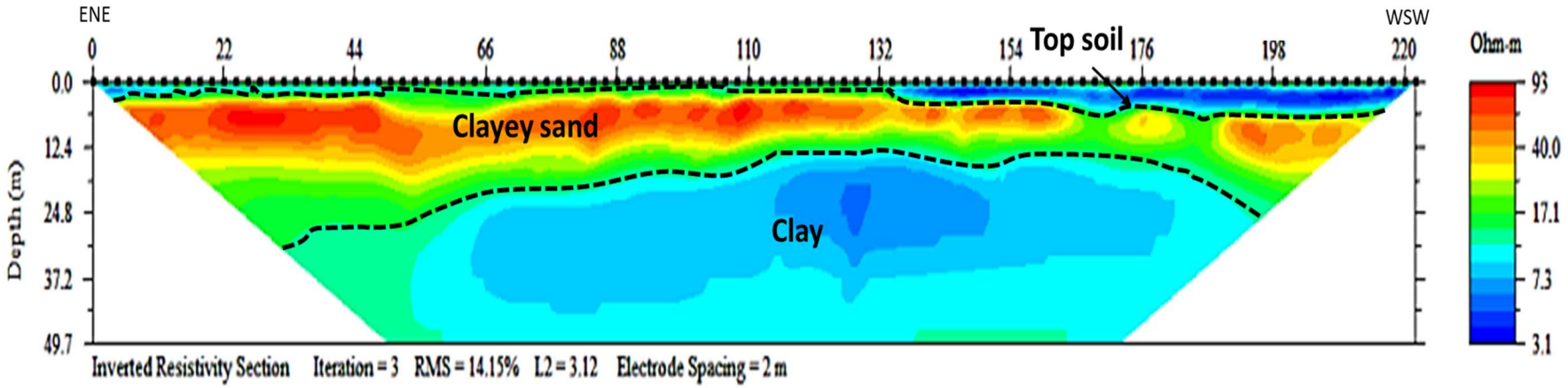

Figure 4.5(c): 2D Electrical Resistivity Inverted section along Profile 3

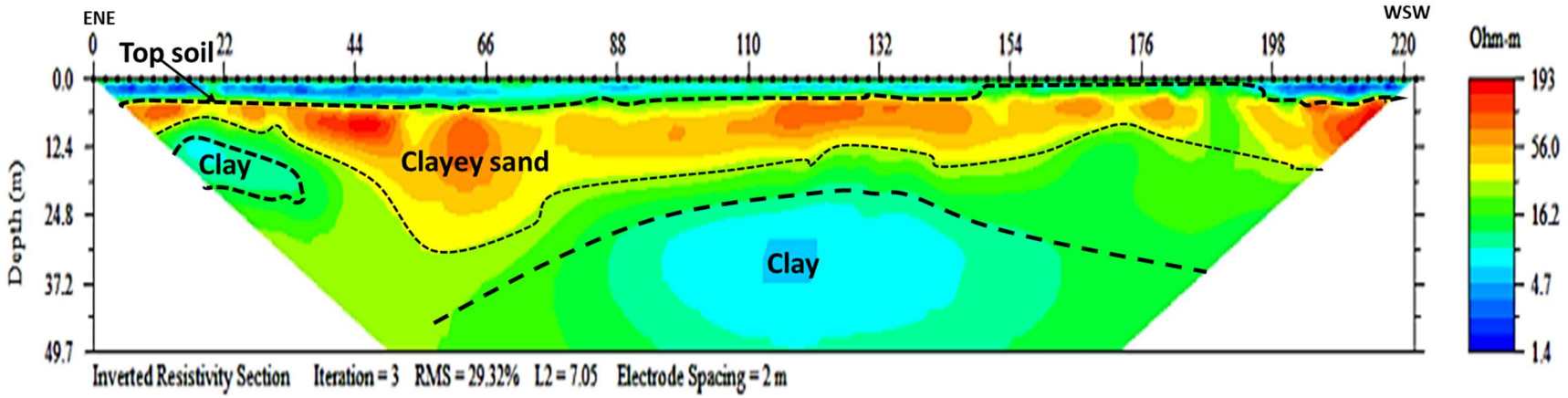

Figure 4.5(d): 2D Electrical Resistivity Inverted section along Profile 4

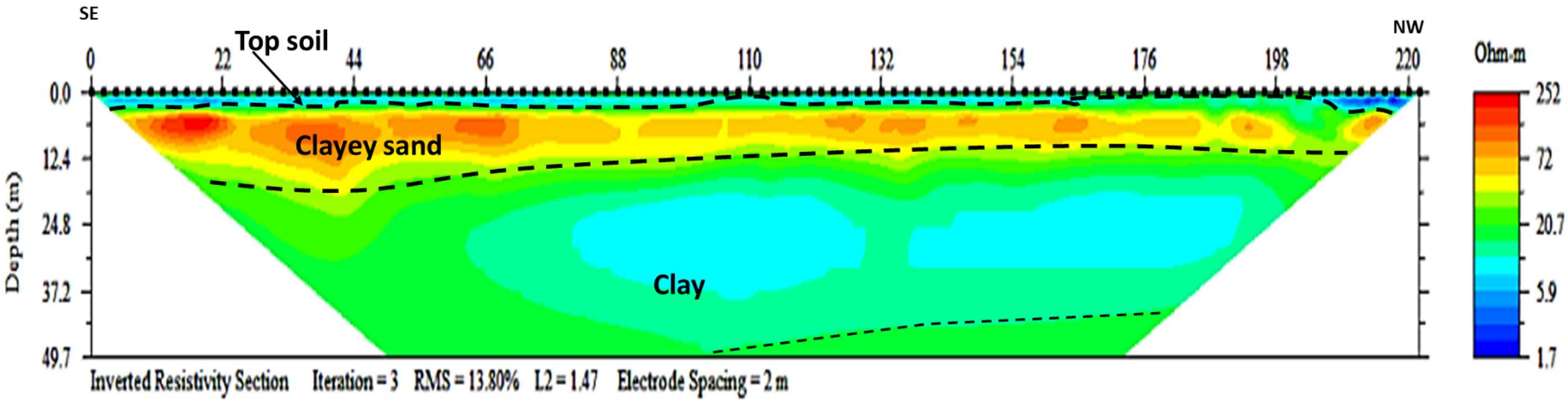

Figure 4.5(e): 2D Electrical Resistivity Inverted section along Profile 5

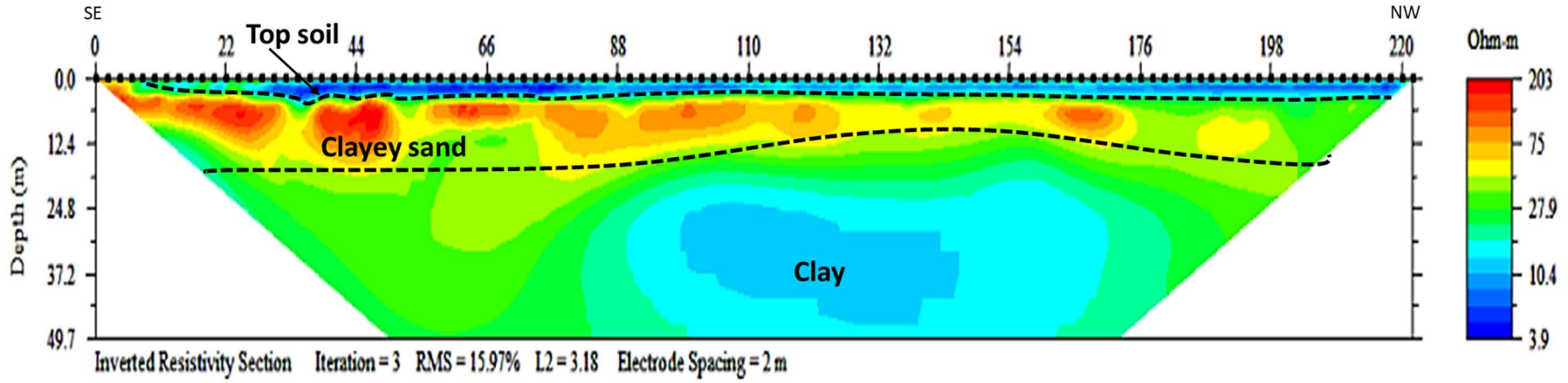

Figure 4.5(f): 2D Electrical Resistivity Inverted section along Profile 6

4.3.2 Traverse 2 (Figure 4.5 (b))

This is also an ENE-WSW trending profile. The top soil resistivity is between 2 and 25 ohm-m and the thickness is roughly 5 m along the whole profile. The second layer has a relatively higher resistivity than the topsoil. The resistivity varied between 34 to 220 ohm-m, and thickness between 6 and 30 m. This layer, interpreted as clayey sand, is thickest at the regions labelled “A” and “B” which seems to be a river channel filled-up with the clayey sand deposit. The third layer is a low resistivity layer of clay whose thickness ranged from about 10 m to over 30 m around the eastern (ENE) end.

A fourth layer having a relatively higher resistivity than the overlying layer was observed at the western end of the traverse. The total depth imaged by the 2D inverted section is 49.7 m. VES 1 is located at 186 m from the start of the profile (figure 4.4(b)). The topsoil and the underlying clay layer from the VES were merged as the topsoil on the 2D inverted section. The thickness of the clayey sand layer as given by VES 1 (i.e. 9 m) was about the same on the 2D inverted section as well.

4.3.3 Traverse 3 (Figure 4.5 (c))

This is another ENE-WSW trending profile. The top soil resistivity is between 3 and 32 ohm-m and the thickness varied between 1 and 6 m along the whole profile. The second layer has a relatively higher resistivity than the topsoil. The resistivity varied between 32 and 92 ohm-m, and thickness between 6 and 15 m. The third layer is a low resistivity layer of clay. The total depth imaged by the 2D inverted section is 49.7 m. VES points 2 and 3 are located at 198 m and 60 m from the start of the profile respectively (figure 4.4(c)).

4.3.4 Traverse 4 (Figure 4.5 (d))

The profile trends in the ENE-WSW direction. The top soil resistivity is between 1 and 12 ohm-m and the thickness varied between 0.5 and 4.5 m along the whole profile. The second layer has a relatively higher resistivity than the topsoil. The resistivity varied between 30 and 193 ohm-m, and thickness between 6 and 20 m. The third layer is a low resistivity layer of clay. The total depth imaged by the 2D inverted section is 49.7 m.

VES point 5 is proximal to the eastern section of Traverse 4 (figure 4.4(d)). Topsoil and the first clay layer delineated by VES 5 were merged together as topsoil on the 2D inverted section. The clayey sand layer which is just 2.1 m thick on the VES was found to be over 20 m on 2D inverted section. Immediately underlying the 2.1 m thick layer of clayey sand on the VES is a low resistivity clay layer (Table 4.1). This suggests that though, the clayey sand was very thick (over 20 m) on the 2D inverted section, the whole clayey sand layer on the 2D inverted section could in reality be intercalation of clayey sands and thin clay beds which merged together on the 2D to give an impression of a very thick clayey sand layer.

4.3.5 Traverse 5 (Figure 4.5 (e))

This is a NW-SE trending profile. The top soil resistivity is between 2 and 15 ohm-m and the thickness varied between 0.5 and 3 m along the whole profile. As in other profiles, the second layer has a relatively higher resistivity than the topsoil. The resistivity varied between 39 and 252 ohm-m, and thickness between 3 and 15 m. The third layer is a low resistivity layer of clay. The total depth imaged by the 2D inverted section is 49.7 m.

4.3.6 Traverse 6 (Figure 4.5 (f))

This is also a NW-SE trending profile. The top soil resistivity is between 4 and 20 ohm-m and the thickness varied between 0 and 3 m along the whole profile. As in other profiles, the second layer has a relatively higher resistivity than the topsoil. The resistivity varied between 40 and 203 ohm-m, and thickness between 6 and 18 m. The third layer is a low resistivity layer of clay. The total depth imaged by the 2D inverted section is 49.7 m

4.4 The 2D Seismic Refraction Tomography

2D seismic refraction tomography was conducted on traverses 3, 4 and 5 with the start of line coinciding with that of 2D electrical resistivity imaging (Figure 3.1). Being just about 140 m long, the 2D seismic tomography lines were shorter than the 2D electrical resistivity imaging lines. The 2D seismic tomography images are shown in figures 4.6 (a), (b) and (c).

4.4.1 Traverse 3 (Figures 4.6 (a))

This profile trends in the ENE-WSW direction. Two layers were delineated on the 2D seismic inverted tomogram. Depth to the second layer varied between 5 and 10 m along the profile (figure 4.6(a)). Since the VES and lithologic log models (Sections 4.1 and 4.1.1) delineated four (4) to five (5) geologic layers in this area, it can be understood that some geologic layers were hidden on the seismic tomogram due to the problem of velocity inversion and this has made the seismic refraction method not very suitable for the delineation of the geologic sequences in the area. The primary wave velocity (V_p) varied between 511 to 1042 ms^{-1}, and 1042 and 1200 ms^{-1} for the first and second layers respectively.

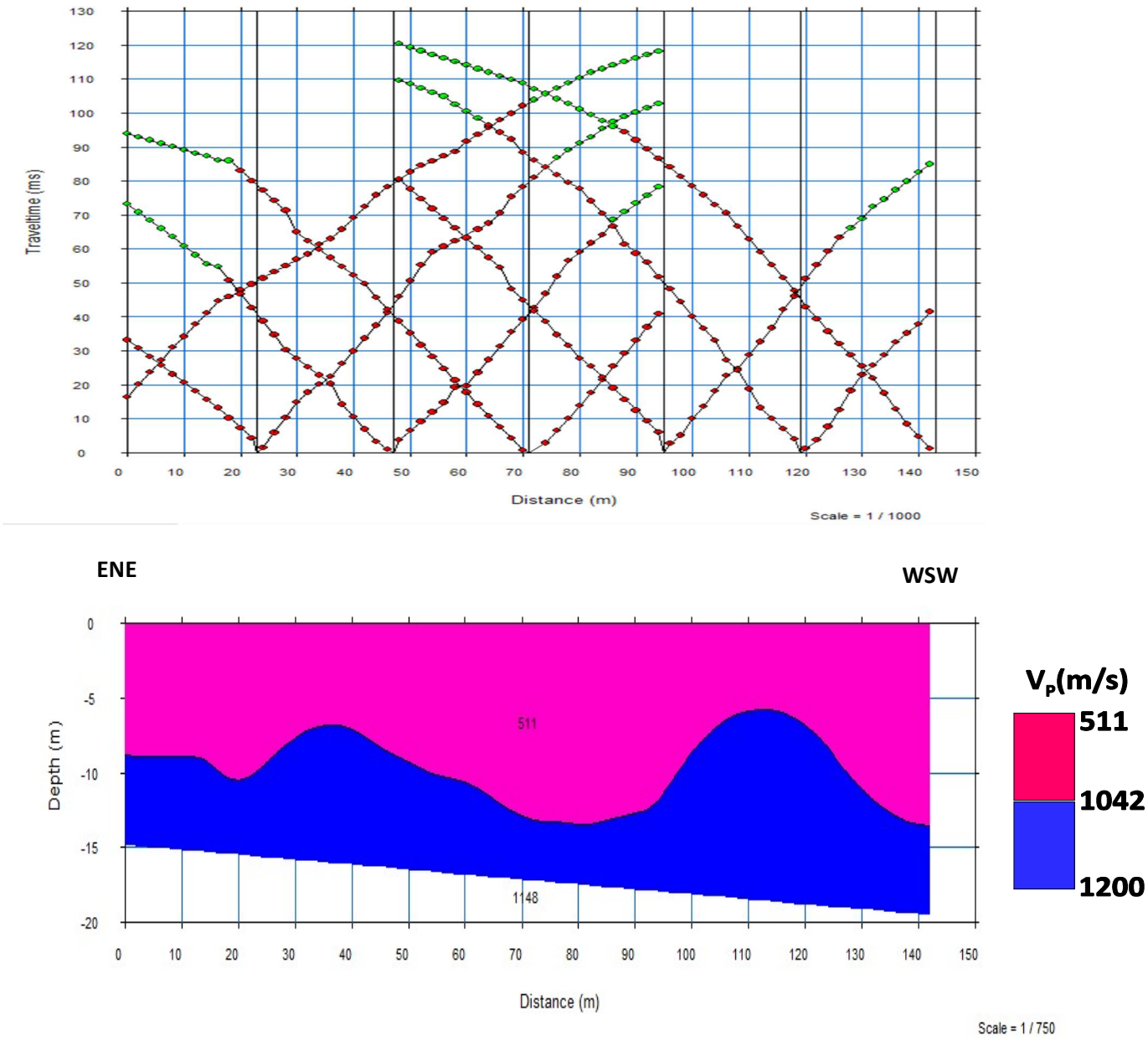

Figure 4.6(a): 2D Seismic Refraction Tomogram along Profile 3

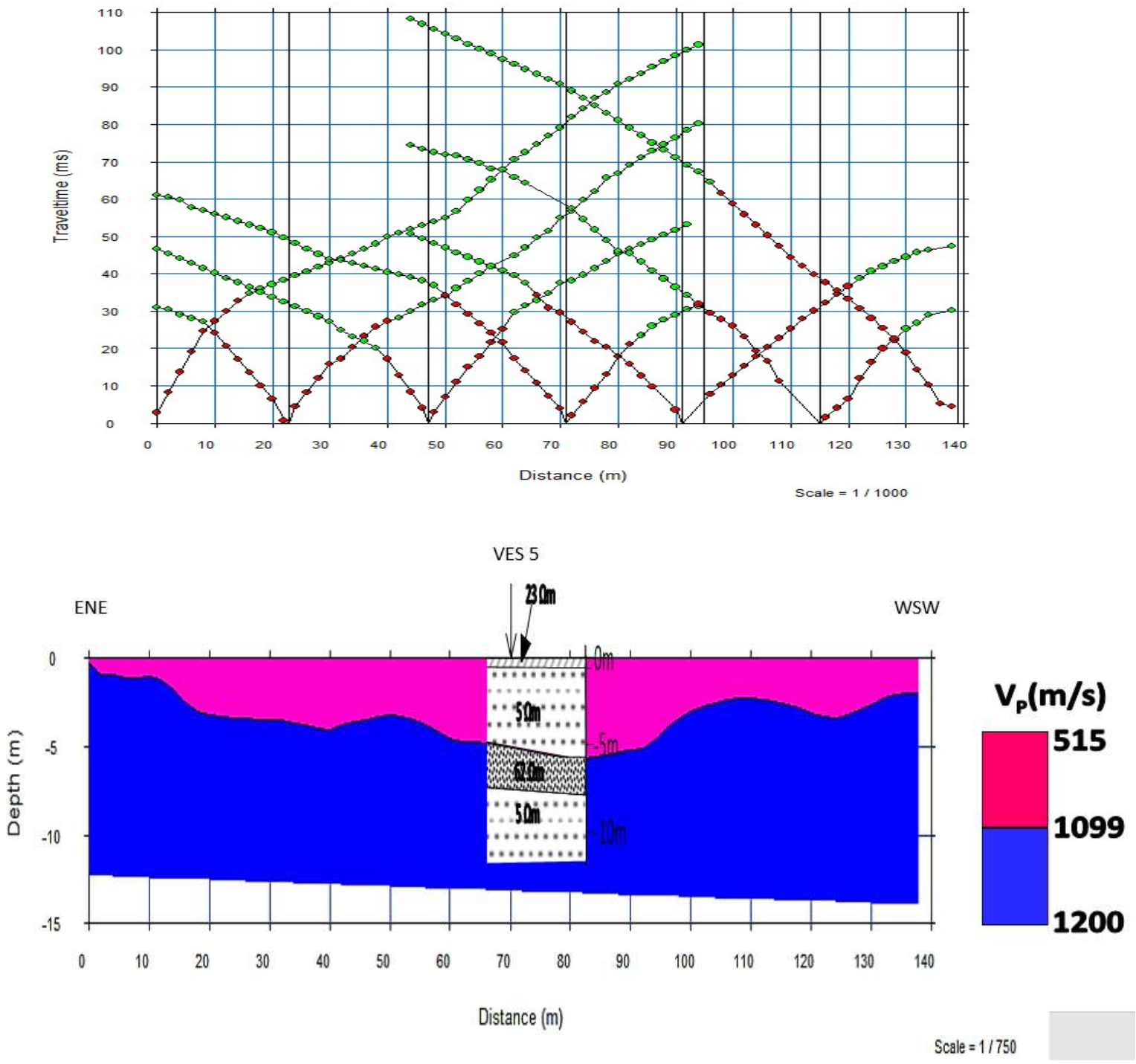

Figure 4.6(b): 2D Seismic Refraction Tomogram along Profile 4

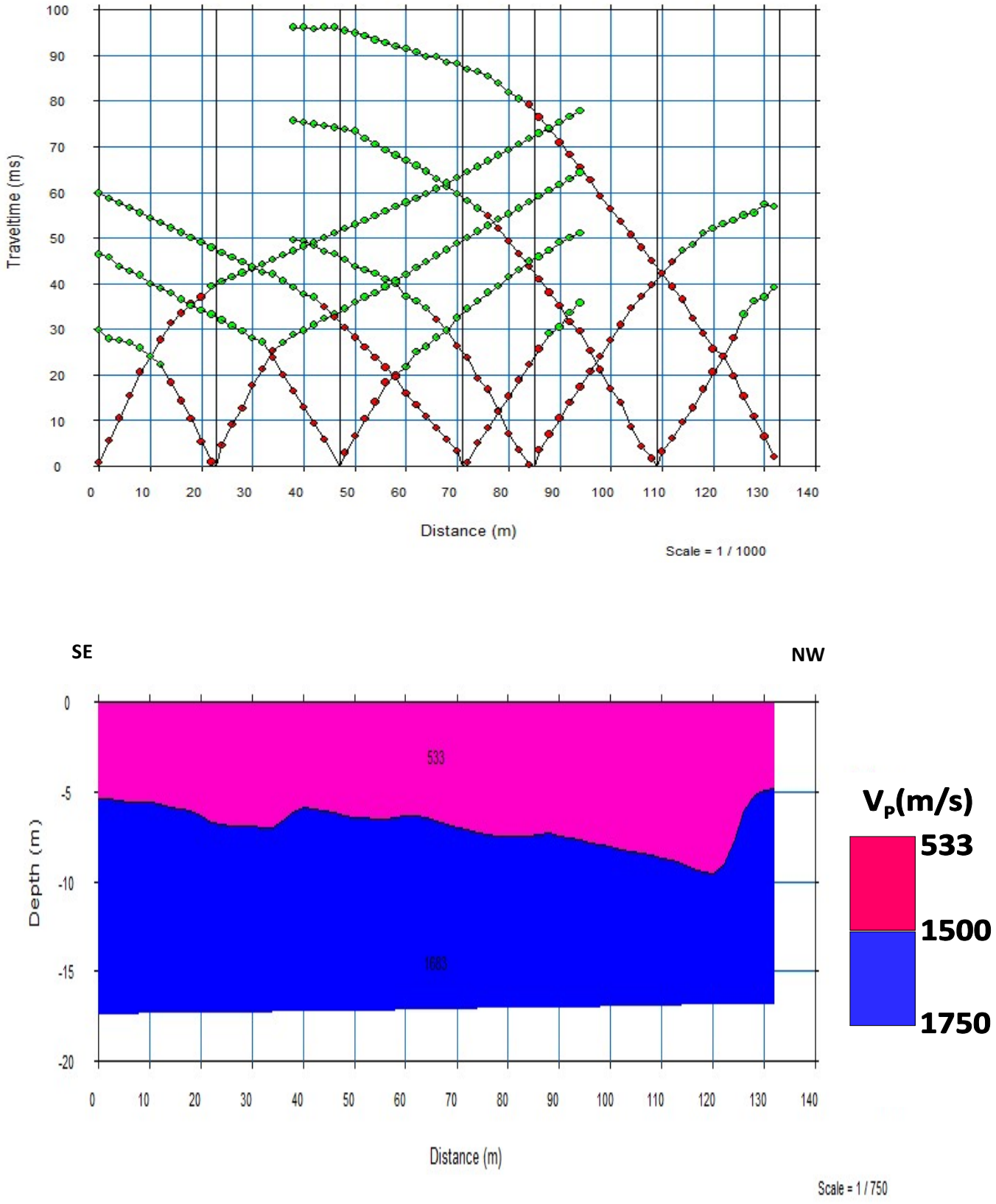

Figure 4.6(c): 2D Seismic Refraction Tomogram along Profile 5

4.4.2 Traverse 4 (Figures 4.6 (b))

This profile also trends in the ENE-WSW direction. Two layers were delineated as well on the 2D seismic tomogram. Depth to the second layer varied between 1 and 5 m along the profile (figure 4.6(b)). VES point 5 is located at exactly 71 m from the start of the profile. When the VES section at VES point 5 was correlated with the seismic refraction tomogram, it was discovered that the first two layers delineated by the VES were merged together as the first layer of the seismic tomogram while the last two layers were also merged together and correspond to the second layer on the seismic tomogram. The primary wave velocity (V_p) varied between 515 to 1099 ms^{-1}, and 1099 and 1200 ms^{-1} for the first and second layers respectively. Being less consolidated based on the range of velocity of propagation of the primary seismic wave (V_p), the first layer is more likely to be constituted of less consolidated sediments that may have been transported with flood current, the study area being part of the flood plain where overflown dam water are discharged.

4.4.3 Traverse 5 (Figures 4.6 (c))

This profile trends in the NW-SE direction. Two layers were also delineated on the 2D seismic image. Depth to the second layer varied between 5.5 and 9.5 m along the profile (figure 4.6(c)). The primary wave velocity (V_p) varied between 533 to 1500 ms^{-1}, and 1500 and 1750 ms^{-1} for the first and second layers respectively. The degree of consolidation of earth material is likely to have played the most significant role in discriminating the layers on the seismic tomogram.

4.5 The Multi-channel Analysis of Surface Wave (MASW) Result

Multi-channel analysis of surface wave data was acquired along the profiles on which 2D seismic refraction tomography data were acquired (Figures 4.7 (a), (b) and (c)). This method makes use of surface waves (i.e. Rayleigh waves) to delineate lithologies and to give an estimate of the shear

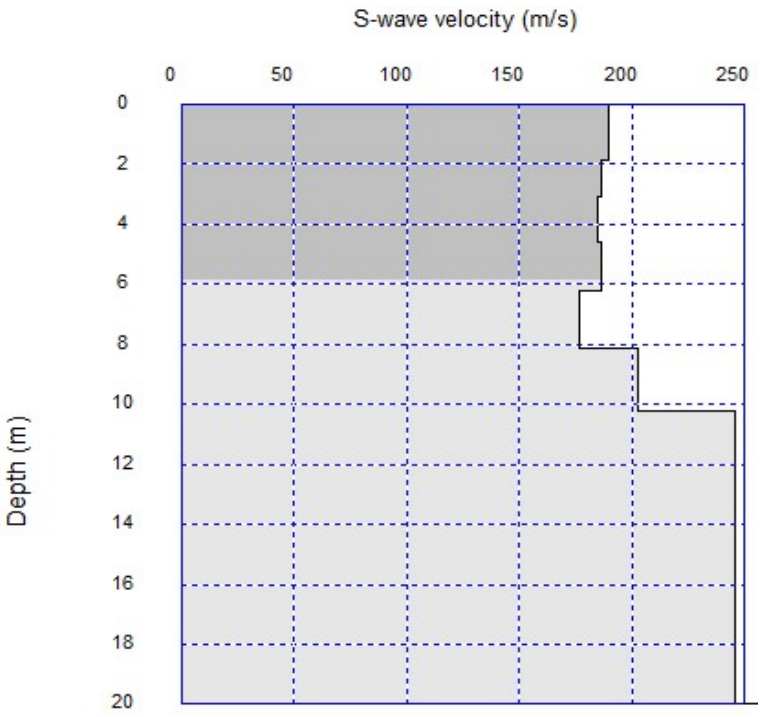

Figure 4.7(a): Shear Wave Velocity Model along Profile 3

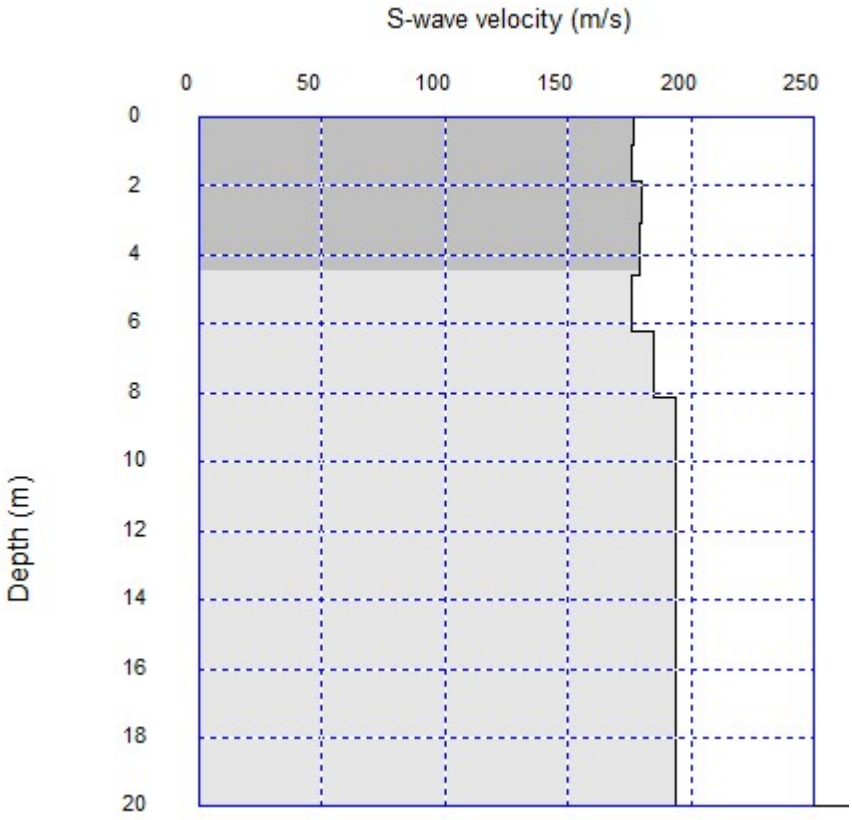

Figure 4.7(b): Shear Wave Velocity Model along Profile 4

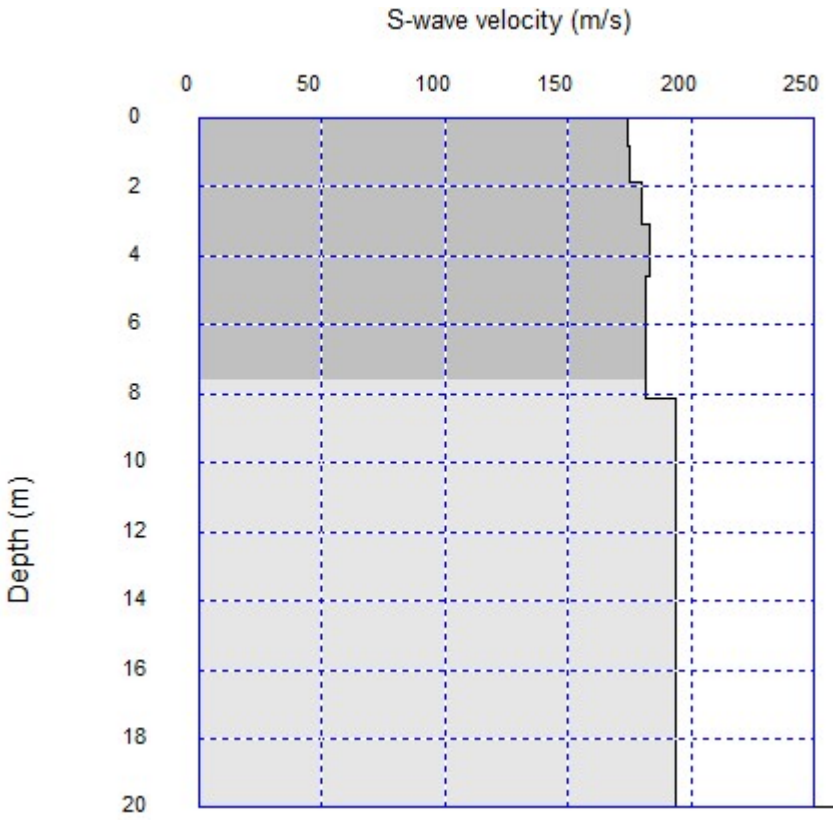

Figure 4.7(c): Shear Wave Velocity Model along Profile 5

wave velocity (Vs). From this method, two geologic layers were delineated along all the three profiles and their shear wave velocities were estimated.

4.5.1 Traverse 3 (Figures 4.7 (a))

This profile trends in the ENE-WSW direction. Of the two layers delineated, the first layer has an average Vs of 185 ms^{-1} while the second layer has an average Vs of 230 ms^{-1} (Figure 4.7 (a)). Average thickness of the first layer is about 5.9 m. This is consistent with the thickness of the first three geoelectric layers of VES 3 (i.e 5.8 m) which is 60 m from the start of the profile on the assumption that the first three layers on the VES was merged together as the first layer of the inverted S-wave model.

4.5.2 Traverse 4 (Figures 4.7 (b))

This profile also trends in the ENE-WSW direction. Of the two layers delineated, the first layer has an average Vs of 175 ms^{-1} while the second layer has an average Vs of 240 ms^{-1} (Figure 4.7 (b)). Average thickness of the first layer is about 4.4 m on this profile.

4.5.3 Traverse 5 (Figures 4.7 (c))

This is a NW-SE trending profile. Of the two layers delineated, the first layer has an average Vs of 175 ms^{-1} while the second layer has an average Vs of 235 ms^{-1} (Figure 4.7 (a)). Average thickness of the first layer is about 7.6 m. VES 5 is located at 86 m from the start of this profile. When compared with VES 5 results, the first layer (delineated on the MASW S-wave model) is thought of as consisting of the first three geoelectric layers of VES 5. These three layers have a combined thickness of 6.6 m.

4.6 Computed Bulk Density (ρ), Compressibility (β), Bulk Modulus (K), Dynamic Shear Modulus (G) and Rock mass Quality (Q) from the Compressional Wave Velocity (Vp) and Shear Wave Velocity (Vs).

Presented in Table 4.2 are the engineering parameters derived from the compressional wave and the shear wave velocities of earth materials in the study area. These parameters include the bulk density (ρ), the compressibility (β), inverse of the compressibility which is usually referred to as the bulk modulus (K), Dynamic Shear Modulus (G) and the Rock Mass Quality (Q). All the computed engineering parameters which are very low indicated that the soil highly incompetent for engineering structures.

Table 4.2: Engineering Parameters Computed from the Vp and Vs of the Subsurface Layers in the Study Area

	V_p Layer 1 (ms^{-1})	**V_p Layer 2 (ms^{-1})**	**V_s Layer 1 (ms^{-1})**	**V_s Layer 2 (ms^{-1})**	**ρ Layer 1 (g/cm^3)**	**ρ Layer 2 (g/cm^3)**	**β Layer 1 (x 10^{-6}Pa)**	**β Layer 2 (x 10^{-6}Pa)**	**K Layer 1 (x 10^6Pa)**	**K Layer 2 (x 10^6Pa)**	**G_{av} Layer 1 (Pa)**	**G_{av} Layer 2 (Pa)**	**Rock-mass Quality (Q) Layer 1**	**Rock-mass Quality (Q) Layer 2**
Profile 3	511 – 1042	1042 – 1200	185	230	1.474 - 1.761	1.761 - 1.825	0.546 - 3.150	0.400 - 0.546	0.318 – 1.832	1.832 – 2.499	55362	96519	0.001026 – 0.003483	0.003483 – 0.005012
Profile 4	515 - 1099	1099 - 1200	175	240	1.477 - 1.785	1.785 - 1.825	0.480 - 3.018	0.402 - 0.480	0.331 – 2.083	2.083 – 2.487	49944	105094	0.001035 – 0.003972	0.003972 – 0.005012
Profile 5	533 – 1500	1500 – 1750	175	235	1.490 - 1.929	1.929 - 2.005	0.235 - 2.760	0.167 – 0.235	0.362 – 4.262	4.262- 5.993	52349	110728	0.001079 – 0.01	0.01 – 0.01778

CHAPTER FIVE

5.1 Summary and Conclusion

Geophysical methods have been used to investigate the competence of the near surface soil at Mountain Top University's permanent site in Makogi-Oba, via Ibafo, Lagos-Ibadan Expressway, Ogun State, Nigeria with a view to determining its suitability for construction purposes.

From the study, it was found out that the area is underlain by a lithologic sequence of clayey topsoil, low resistivity clay layer, relatively high resistivity clayey sand layer, and another low resistivity clay layer. On the 2D ERT inverted sections, the upper first two lithologic layers were merged together as a clayey topsoil which was underlain by a relatively high resistivity clayey sand which in turn was underlain by a thick column of low resistivity clay layer. The clayey sand layer is the most competent of the lithologic sequence delineated. The seismic refraction tomography and MASW delineated two layers which were likely discriminated based on their relative degree of consolidation.

The clayey sand layer, which is the most competent lithologic sequence, has apparent electrical resistivity values ranging from 13 to 163 ohms-m, and thickness ranging from 1.6 to 9.1 m from 1D VES models. The thickness obtained for this layer on the 2D ERT inverted sections is about 6m on the average though there is possibility of thickness overestimation due to merging of adjacent layers. The depth to this layer ranged from 2.2 to 5.8 m using the 1D VES layer. The topsoil in the study area is generally not suitable for engineering or construction purpose.

5.2 Recommendation

From the results of the geophysical investigations, a pile foundation is recommended for buildings or construction works that would be undertaken in this area. The pile should be anchored on the

clayey sand layer. The depth to this layer is between 2.2 to 5.8 m. More VES data can be acquired so that a more representative isopach map and map of the depth to this clayey sand layer can be generated.

It should be noted however that before any construction of any sort should be done at this site, the mechanism to take care of flooding that occurs when the Ogun river dam is spilled out should be put in place. Water marks on shipping containers found within the site indicated that the flood level could reach close to 2 m. Owing to this fact, construction is discouraged until probably the area is sand-filled to about 2.5 m higher, and river channels dredged so that flood can have free channels to pass when the dam is spilled.

REFERENCES

Adeleke, B.O. and Leong, G. C. (1978). Certificate Physical and Human Geography, West African Ed. Oxford University Press, Nigeria, Ibadan. pp. 32

Adepelumi, A.A. and Olorunfemi, M.O. (2000). "Engineering Geological and Geophysical Investigation of the reclaimed Lekki Peninsula, Lagos, SW, Nigeria". *Bulletin of Engineering Geology and the Environment*, 58: 125-132.

Adewunmi, I. and Olorunfemi, M.O. (2005). "Using Geoinformatics in Construction Management". *Journal of Applied Sciences*, 5 (4): 761-767.

Akintorinwa, O.J. and Adeusi, F.A. (2009). "Integration of Geophysical and Geotechnical Investigation for a Proposed Lecture Room Complex at the Federal University of Technology, Akure, SW, Nigeria". *Ozean Journal of Applied Sciences* 2(3): 105-118.

Ayolabi, E.O., Folorunso, A. F. and Jegede, O.E. (2012). "An application of 2D Electrical Resistivity Tomography in Geotechnical Investigations of Foundation defects: a case study". *Journal of Geology and Mining Research,* 3(12): 142-151.

Bhattacharya, P.K. and Patra, H.P. (1968). "Direct Current Electric Sounding (Methods in Geochemistry and Geophysics, 9.)". *Elsevier Publishing Co.*, Amsterdam, London, New York, 106(2), 135 p.

de Klasz, I. and Jan Du Chene, R. (1978). "Presence of Albian-Cenomanian in South-western Nigeria and Its Paleogeographic Implications". Compte Rendu de la Société de Physique et d'Histoire *Naturelle de Genève*, 13, 10-15.

Elawadi, E., El-Qady, G, Nigm, A., Shaaban, F. and Ushijima, K. (2006). Integrated Geophysical Survey for Site Investigation at a New Dwelling Area, Egypt. *Journal of Environmental and Engineering Geophysics,* 11(4): 249-259.

Gardner, G.H.F., Gardner, L.W., and Gregory, A.R. (1974). "Formation velocity and density—the diagnostic basics for stratigraphic traps." Geophysics 39:770–780, pp.

Google Maps (2020). Mountain Top University Permanent Site, Makogi-Oba, Ogun State, Nigeria, 1:1500. *Google Maps Online*. Accessed 21 November, 2020.

Kearey, P., Brooks, M., and Hill, I. (2002). "An introduction to geophysical exploration (3rd ed.)". *Blackwell Publishing*, Malden, U.S.A. 281 p.

Loke, M.H. (2002). "Electrical imaging surveys for environmental and engineering studies: A practical guide to 2-D and 3-D surveys". 127 p.

Lowrie, W. (2007). Seismic wave propagation. In: Lowrie W. (2nd Ed.). Fundamentals of Geophysics. Cambridge University Press, 171-192, pp.

Momoh, L.O., Akintorinwa, O., and Olorunfemi, M.O. (2008). "Geophysical Investigation of Highway Failure – A Case study from the Basement Complex Terrain of Southwestern Nigeria". *Journal of Applied Sciences*, 4(6): 637-648.

McDowell, P.W., Barker, R.D., and Butcher A.P. (2002). "Geophysics in engineering investigations". London: *Construction Industry Research and Information Association*, CIRIA C562

Omatsola, M.E. and Adegoke, O.S. (1981). "Tectonic Evolution and Cretaceous Stratigraphy of the Dahomey Basin. *Journal of Mining and Geology,* 18: 130-137.

Petters, S.W (1982). Central West African Cretaceous – Tertiary benthic foraminifera and stratigraphy: Paleontographical Abseiling v. 179, 1-104.

Reynolds, J.M. (1997). "An Introduction to Applied and Environmental Geophysics". Chichester: John Wiley and Sons Ltd. pp. 769

Reynolds, J.M. (2011). "Electrical resistivity sounding and tomography". Technical Summary. Reynolds International. 2, pp. 2

USGS (2006) Shuttle radar topography mission, 1 Arc second scene, filled-finished-B, global land cover facility. Maryland: University of Maryland, College Park.

Taipodia, J., and Dey, A. (2012). "A review of Active and Passive MASW Techniques". *Engineering Geophysics for Civil Engineering and Geo-Hazards,* National Workshop CBRI, Roorkee pp. 1-13

Telford, W.M., L.P. Geldart, R.E. Sheriff, and D.A. Keys, (1990). "Applied Geophysics". Cambridge University Press. 744p.

Yilmaz, (2001). "Seismic data analysis". Processing, Inversion, and Interpretation of Seismic Data. *Society of Exploration Geophysicists,* 1, 41-46, pp.

Internet Resources

https://www.en.climate-data.org/africa/nigeria/lagos/lagos-552/ Retrieved on 31st November, 2020

https://www.lagosstate.gov.ng/about-lagos/ Retrieved on 31st November, 2020

APPENDIX

Resistivity (VES) Data Sheets

Date: 13th January 2021 Observer: Geosciences Department

Electrode Array: Schlumberger Instrument: AGI Supersting R1

Site Location: MTU Permanent Site Geographic Coordinates:

Station Location: VES 1 Northing: 745927.00 m N

Easting: 542201.00 m E

Electrode Position	AB/2	MN/2	Pi (AB/2 Squad.)	K	R	Rho
1	1	0.25	3.141592654	6.283185307	6.080	38.20
2	2	0.25	12.56637061	25.13274123	0.597	15.00
3	3	0.25	28.27433388	56.54866776	0.177	10.00
4	4	0.25	50.26548246	100.5309649	0.075	7.50
5	6	0.25	113.0973355	226.1946711	0.031	7.00
6	6	0.50	113.0973355	113.0973355	0.062	7.00
7	9	0.50	254.4690049	254.4690049	0.295	75.00
8	12	0.50	452.3893421	452.3893421	0.019	8.50
9	15	0.50	706.8583471	706.8583471	0.013	9.00
10	15	1.00	706.8583471	353.4291735	0.025	9.00
11	20	1.00	1256.637061	628.3185307	0.014	9.00
12	25	1.00	1963.495408	981.7477042	0.008	8.00
13	32	1.00	3216.990877	1608.495439	0.004	7.00
14	40	1.00	5026.548246	2513.274123	0.002	6.00
15	40	2.50	5026.548246	1005.309649	0.006	6.00
16	50	2.50	7853.981634	1570.796327	0.003	5.00

Station Location: VES 2 Geographic Coordinates:

Northing: 745988 m N

Easting: 542186 m E

Electrode Position	AB/2	MN/2	Pi(AB/2 Squ.)	K	R	Rho
1	1	0.25	3.141593	6.283185	1.751	11.00
2	2	0.25	12.56637	25.13274	0.199	5.00
3	3	0.25	28.27433	56.54867	0.071	4.00
4	4	0.25	50.26548	100.531	0.040	4.00
5	6	0.25	113.0973	226.1947	0.019	4.20
6	6	0.5	113.0973	113.0973	0.035	4.00
7	9	0.5	254.469	254.469	0.024	6.00
8	12	0.5	452.3893	452.3893	0.015	7.00
9	15	0.5	706.8583	706.8583	0.011	8.00
10	15	1	706.8583	353.4292	0.023	8.00
11	20	1	1256.637	628.3185	0.016	10.00
12	25	1	1963.495	981.7477	0.011	11.00
13	32	1	3216.991	1608.495	0.007	11.00
14	40	1	5026.548	2513.274	0.004	10.00
15	40	2.5	5026.548	1005.31	0.010	10.00

Station Location: VES 3 Geographic Coordinates:

Northing: 745996 m N

Easting: 542322 m E

Electrode Position	AB/2	MN/2	Pi(AB/2 Squ.)	K	R	Rho
1	1	0.25	3.141593	6.283185	1.862	11.70
2	2	0.25	12.56637	25.13274	2.626	66.00
3	3	0.25	28.27433	56.54867	0.133	7.50
4	4	0.25	50.26548	100.531	0.104	10.50
5	6	0.25	113.0973	226.1947	0.044	10.00
6	6	0.5	113.0973	113.0973	0.133	15.00
7	9	0.5	254.469	254.469	0.079	20.00
8	12	0.5	452.3893	452.3893	0.053	24.00
9	15	0.5	706.8583	706.8583	0.035	25.00
10	15	1	706.8583	353.4292	0.081	28.50
11	20	1	1256.637	628.3185	0.049	31.00
12	25	1	1963.495	981.7477	0.035	34.00
13	32	1	3216.991	1608.495	0.022	36.00
14	40	1	5026.548	2513.274	0.014	36.00
15	40	2.5	5026.548	1005.31	0.038	38.00
16	50	2.5	7853.982	1570.796	0.000	

Station Location: VES 4

Geographic Coordinates:

Northing: 746032.00 m N

Easting: 542302.00 m E

Electrode Position	AB/2	MN/2	Pi (AB/2 Squad.)	K	R	Rho
1	1	0.25	3.141593	6.283185	1.926	12.10
2	2	0.25	12.56637	25.13274	0.374	9.40
3	3	0.25	28.27433	56.54867	0.182	10.30
4	4	0.25	50.26548	100.531	0.129	13.00
5	6	0.25	113.0973	226.1947	0.084	19.00
6	6	0.5	113.0973	113.0973	0.018	2.00
7	9	0.5	254.469	254.469	0.104	26.50
8	12	0.5	452.3893	452.3893	0.071	32.00
9	15	0.5	706.8583	706.8583	0.052	37.00
10	15	1	706.8583	353.4292	0.108	38.00
11	20	1	1256.637	628.3185	0.068	43.00
12	25	1	1963.495	981.7477	0.045	44.00
13	32	1	3216.991	1608.495	0.025	40.00
14	40	1	5026.548	2513.274	0.015	38.00
15	40	2.5	5026.548	1005.31	0.039	39.00
16	50	2.5	7853.982	1570.796	0.022	34.90

Station Location: VES 5

Geographic Coordinates:

Northing: 746080 m N

Easting: 542186 m E

Electrode Position	AB/2	MN/2	Pi(AB/2 Squ.)	K	R	Rho
1	1	0.25	3.141592654	6.283185	2.387	15.00
2	2	0.25	12.56637061	25.13274	0.298	7.50
3	3	0.25	28.27433388	56.54867	0.106	6.00
4	4	0.25	50.26548246	100.531	0.055	5.50
5	6	0.25	113.0973355	226.1947	0.024	5.50
6	6	0.5	113.0973355	113.0973	0.049	5.50
7	9	0.5	254.4690049	254.469	0.024	6.20
8	12	0.5	452.3893421	452.3893	0.017	7.50
9	15	0.5	706.8583471	706.8583	0.013	9.00
10	15	1	706.8583471	353.4292	0.025	9.00
11	20	1	1256.637061	628.3185	0.016	10.00
12	25	1	1963.495408	981.7477	0.010	10.00
13	32	1	3216.990877	1608.495	0.006	9.00
14	40	1	5026.548246	2513.274	0.003	8.00
15	40	2.5	5026.548246	1005.31	0.008	8.50
16	50	2.5	7853.981634	1570.796	0.004	7.00